New constraints on the charged Higgs sector in two-Higgs-doublet models

V. Barger and J. L. Hewett
Physics Department, University of Wisconsin, Madison, Wisconsin 53706

R. J. N. Phillips
Rutherford Appleton Laboratory, Chilton, Didcot, Oxon, England
(Received 20 December 1989; revised manuscript received 6 February 1990)

Two-Higgs-doublet models predict nonstandard physical effects through the interactions of charged Higgs scalars. We analyze the experimental measurements that bound these effects and quantify the resulting constraints on the charged-Higgs-boson mass and coupling parameter $\tan\beta$. We consider low-energy data relating to B_d^0-$\bar{B}_d^0$, D^0-$\bar{D}^0$, and K^0-$\bar{K}^0$ mixing, and high-energy measurements at $p\bar{p}$ colliders relating to searches for the top quark and events with large missing E_T. Our analysis systematically takes account of theoretical uncertainties in bag factors, decay constants, and quark mixing matrix elements by Monte Carlo sampling. We combine our results to determine the regions in the charged-Higgs-boson parameter space that are consistent with present data. An important result is that the Collider Detector at Fermilab top-quark mass bound $m_t > 77$ GeV can probably not be evaded by appealing to $t \to bH^+$ decays, since only a very small sliver of parameter space is consistent with $m_t < 77$ GeV in this scenario. Consistency with either the CERN NA31 or Fermilab E731 ϵ'/ϵ measurements is possible. The rare decays $B \to K^*\gamma$, $K^+ \to \pi^+ \nu\bar{\nu}$, and $K_L \to \mu\mu$ are also examined in these models within the context of our combined analysis.

I. INTRODUCTION

The standard model (SM) of electroweak interactions has been remarkably successful in describing physics below the Fermi scale and is in complete agreement[1] with all experimental data. However, the Higgs sector has remained elusive, and there exists no experimental information on its nature. The possibility of an enlarged Higgs sector beyond the minimal one-doublet version of the SM (Ref. 2) is thus consistent with data and has received substantial attention in the literature. The simplest extensions are models with two Higgs doublets (requiring the existence of charged Higgs bosons) which are present in many scenarios beyond the SM, including supersymmetry[3] (SUSY), Peccei-Quinn models,[4] spontaneous CP violation,[5] and E_6 superstring-inspired theories.[6] Because of the lack of direct experimental knowledge, it is prudent to combine all information on the indirect effects of charged Higgs bosons in order to place constraints on this sector. In this paper we focus on possible charged-Higgs-boson contributions to low-energy processes, such as B_d^0-$\bar{B}_d^0$ and D^0-$\bar{D}^0$ mixing, Δm_K, and ϵ, as well as the influence of charged Higgs bosons on the top-quark search and missing-E_T measurements at $p\bar{p}$ colliders. The results from this combined analysis are then used to restrict the parameters in the charged Higgs sector and determine the region which is consistent with all data. We then make predictions for the charged-Higgs-boson contributions to ϵ'/ϵ and the rare decays $K_L \to \mu\mu$, $K^+ \to \pi^+ \nu\bar{\nu}$, and $B \to K^*\gamma$.

The phenomenology of charged Higgs bosons has been previously considered.[7-15] However, our present reexamination of possible restrictions that current data may place on the charged Higgs section is well motivated for several reasons.

(i) We perform a simultaneous analysis of several low-energy processes and recent Fermilab Tevatron collider data mentioned above and combine these results to obtain the overall allowed region of parameter space in the charged Higgs sector. Such a comprehensive analysis (in particular, the inclusion of CP violation and $p\bar{p}$ collider data) does not exist in the literature.

(ii) Some of the relevant pieces of experimental data are new; others have either improved or changed substantially since previous studies were performed. As we will see below, the corresponding results are thus significantly different.

(iii) We thoroughly investigate the entire possible range of charged-Higgs-boson and top-quark masses, $m_{H^\pm}$ and m_t, respectively. With the likely possibility of a heavy top quark,[16] the approximation $m_t \ll m_{H^\pm}$ used in early analyses[8] may be invalid. We rederive basic formulas where needed with no approximations, and include the case $m_{H^\pm} < m_t$.

(iv) We fully explore the freedom in the Kobayashi-Maskawa[17] (KM) matrix, as well as the uncertainties in hadronic matrix elements and decay constants using numerical techniques.

In the remainder of this section we give a brief review of the two-Higgs-doublet model. In Sec. II we present the detailed calculations of charged-Higgs-boson contributions to low-energy processes. Using numerical techniques we extensively sample the parameters in the KM matrix and subject them to restrictions from experimental data on the values of the KM matrix elements as well as unitarity considerations. The uncertainties in the ha-

 ©1990 The American Physical Society

dronic matrix elements and decay constants are also thoroughly investigated. We compare our predictions with data for B_d^0-$\bar{B}_d^0$ and D^0-$\bar{D}^0$ mixing, ϵ, and Δm_K, and obtain the range of charged Higgs parameter space which is consistent with low-energy experiment. Using these restrictions we then predict the value of ϵ'/ϵ and the decay rates for $b \to s\gamma$, $K^+ \to \pi^+ \nu\bar{\nu}$, and $K_L \to \mu\mu$ in the two-Higgs-doublet model and compare to the corresponding SM values. In Sec. III we use various bounds from the top-quark search and missing-E_T ($\not{E}_T$) measurements of the Collider Detector at Fermilab (CDF) Collaboration[16] to constrain possible top-quark decays into charged Higgs bosons. We find that the CDF data can be used to rule out large regions of parameter space for $m_t \lesssim 80$ GeV. We then give a brief summary of our conclusions in Sec. IV.

There are several classes of two-Higgs-doublet models which naturally avoid tree-level flavor-changing neutral currents that can be induced by Higgs-boson exchange.[18] One choice, hereafter called model I, is where one doublet ϕ_2 gives masses to all quarks and leptons and the other doublet ϕ_1 essentially decouples from fermions. In a second model (model II) one doublet ϕ_2 gives mass to charge $Q=+\frac{2}{3}$ quarks (and possibly neutrinos) and another doublet ϕ_1 gives mass to charge $Q=-\frac{1}{3}$ quarks and $Q=-1$ leptons. Two other models are also possible (models III and IV) in which the down-type quarks and charged leptons receive mass from different doublets. A summary of which type of fermions couple to ϕ_1 and ϕ_2 in models I–IV is given in Table I. Each doublet obtains a vacuum expectation value (VEV) v_i subject only to the constraint that $v_1^2+v_2^2=v^2$, where v is the usual VEV of the SM. The generic charged Higgs coupling to fermions in models I–IV (assuming massless neutrinos) is given by

$$\mathcal{L}=\frac{g}{2\sqrt{2}M_W}H^{\pm}[V_{ij}m_{u_i}A_u\bar{u}_i(1-\gamma_5)d_j + V_{ij}m_{d_j}A_d\bar{u}_i(1+\gamma_5)d_j + m_l A_l\bar{\nu}(1+\gamma_5)l]+\text{H.c.}\ , \quad (1.1)$$

where the values of the coefficients A_f for all four models are given in Table I; g is the usual $SU(2)_L$ coupling constant, V_{ij} is the relevant element of the KM matrix, and $\tan\beta=v_2/v_1$ is the ratio of VEV's. To compare these couplings in the four models we show the branching fraction $B(H^{\pm}\to\tau\nu)$ as a function of $\tan\beta$ for each model in Fig. 1. The difference in $B(H^+\to\tau\nu)$ between models II and IV is noticeable only for $\tan\beta\gtrsim 2$ and is due to the fact that $m_s\neq 0$. The difference between models I and III becomes large for $\tan\beta\gtrsim 2$ and is due to the fact that the m_s term in model III is proportional to $\tan^4\beta$. Model II is that which is present in SUSY and E_6 theories, and is the model which has gained the most attention in the literature. In this paper we present results for both models I and II. However, we note that the charged-Higgs-boson contributions to processes which depend only on the quark sector (e.g., the processes examined in Sec. II) are the same in models I and IV and in models II and III. Thus our results presented in Sec. II for models I and II also apply for models IV and III, respectively. Similarly, as long as the $m_t\cot\beta$ coupling dominates over the $m_b\tan\beta$ coupling in the $\bar{t}bH$ vertex (i.e., for $\tan\beta\lesssim 2.0$ as seen in Fig. 1) model III is substantially equivalent to model I and model IV is equivalent to model II for the high-energy effects studied in Sec. III.

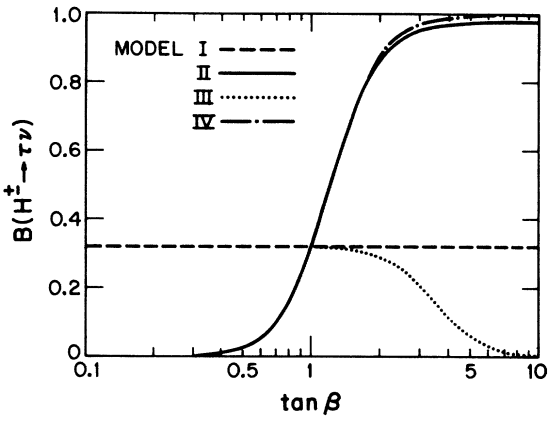

FIG. 1. The branching fraction $B(H^{\pm}\to\tau\nu)$ vs $\tan\beta$ in models I–IV. We take $m_c=1.5$ GeV, $m_s=0.15$ GeV, $m_\tau=1.784$ GeV, $|V_{cs}|=1.0$, and $m_{H^{\pm}}<m_t-m_b$.

The mass $m_{H^{\pm}}$ and the ratio v_2/v_1 are *a priori* free parameters in a general two-doublet model. It has been argued that the inequalities $m_t \gg m_b$ and $m_c \gg m_s$ are not

TABLE I. Summary of which doublet, ϕ_1 or ϕ_2, gives mass to each type of fermion and the values of the coefficients A_f in the charged Higgs coupling to fermions in Eq. (1.1) for models I–IV.

Models	I		II		III		IV	
	VEV	A_f	VEV	A_f	VEV	A_f	VEV	A_f
$\begin{pmatrix} u \\ d \end{pmatrix}$	2	$\cot\beta$	2	$\cot\beta$	2	$\cot\beta$	2	$\cot\beta$
	2	$-\cot\beta$	1	$\tan\beta$	1	$\tan\beta$	2	$-\cot\beta$
$\begin{pmatrix} \nu \\ l \end{pmatrix}$	2	$-\cot\beta$	1	$\tan\beta$	2	$-\cot\beta$	1	$\tan\beta$

due to the Yukawa couplings alone, but suggest[2,6,19] $v_2 > v_1$. This hierarchy occurs naturally from the renormalization-group evolution in supergravity[2] and E_6 superstring-inspired[6] models, but need not be the case in a general two-doublet model. The current experimental bound on the $H^{\pm}$ mass is $m_{H^{\pm}} > 19$ GeV from DESY PETRA (Ref. 20), and it is expected[2] that experiments at KEK TRISTAN will be able to set the limit $m_{H^{\pm}} \gtrsim 25$ GeV. ALEPH (Ref. 21) has recently reported the bounds of $m_{H^{\pm}} > 30$ GeV with a value of $B(H^{\pm} \to cs) = 100\%$ and $m_{H^{\pm}} > 42$ GeV with $B(H^{\pm} \to \tau\nu) = 100\%$. In minimal SUSY models $m_{H^{\pm}}$ is restricted to lie above M_W (Ref. 22), while the bound is less stringent in E_6 superstring models giving $m_{H^{\pm}} > 53$ GeV (Ref. 23). Recent limits[21] on the mass of the SM Higgs boson from ALEPH at CERN can be used[24] together with the mass relationships between the Higgs and gauge bosons in SUSY models to severely constrain $m_{H^{\pm}}$ and $\tan\beta$ in these theories. However, there are no theoretical restrictions on the value of $m_{H^{\pm}}$ and $\tan\beta$ in general two-doublet models.

In principle, constraints on $m_{H^{\pm}}$ can be obtained[2,25] by evaluating the $H^{\pm}$ contributions to the ρ parameter (the ratio of neutral-current-to-charge-current strengths in the effective low-energy Lagrangian). However, in practice, these constraints are quite dependent on the other parameters present in the theory (such as the masses of the neutral Higgs bosons) and are generally very model dependent. In SUSY models, in which there exist particular relationships between the masses of the Higgs and gauge bosons, the charged-Higgs-sector contributions to ρ vary substantially[26] with $\tan\beta$, but are always small giving $|\Delta\rho| \lesssim 10^{-3}$.

Clearly, any constraints on $m_{H^{\pm}}$ and $\tan\beta$ from low-energy and hadron collider data will be strongly dependent on the value of the top-quark mass. If 100% of the t-quark decays proceed through SM charged-current interactions then the existing limits on the top mass are $m_t > 77$ GeV from CDF (Ref. 16), $m_t > 40.7$ GeV from Mark II (Ref. 27), and $m_t > 44.5$ GeV from OPAL (Ref. 28). If the decay $t \to H^+ b$ is possible, the CDF bound is invalidated.[12] Mark II has investigated this potential decay mode and places the lower bound[27] $m_t > 40$ GeV for $m_{H^{\pm}} = 25$ GeV with $B(H^{\pm} \to \tau\nu) < 70\%$ and similarly, OPAL sets the limit[28] $m_t > 45.2$ GeV for $23 \le m_{H^{\pm}} \le 38$ GeV with $B(H^{\pm} \to \tau\nu) = 0$.

One can place some semiquantitative restrictions on $m_{H^{\pm}}$ and $\tan\beta$ by requiring that the $H^{\pm}$ width not be too large and that the $\bar{t}bH$ coupling remain perturbative. It is clear from Eq. (1.1) that the width and $\bar{t}bH$ coupling both grow rapidly with increasing m_t and hence perturbation theory may become endangered for some values of the parameters. If we demand that the theory remain perturbative, a bound on $\tan\beta$ as a function of m_t is obtained. Of course, one should be aware that validity of perturbation theory is not a physical limitation, but it is a limitation on the theoretically accessible region. There are various possible ways to define the boundary of the perturbative region. A simple empirical prescription is to require that Γ/m should not be too large, e.g., $\Gamma/m < \frac{1}{2}$. If $m_{H^{\pm}} > m_t + m_b$ the dominant contribution to the $H^{\pm}$ width is

$$\frac{\Gamma_{H^{\pm}}}{m_{H^{\pm}}} \simeq \frac{3G_F m_t^2}{4\sqrt{2}\pi\tan^2\beta} . \tag{1.2}$$

The requirement that $\Gamma_{H^{\pm}}/m_{H^{\pm}} < \frac{1}{2}$ yields the perturbative boundary

$$\tan\beta \gtrsim \frac{m_t}{500\ \text{GeV}} . \tag{1.3}$$

If $m_t > m_{H^{\pm}} + m_b$ the decay $t \to bH$ is kinematically allowed and the requirement that the t-quark width

$$\frac{\Gamma_t}{m_t} \simeq \frac{G_F m_t^2}{8\pi\sqrt{2}\tan^2\beta} \tag{1.4}$$

not exceed $\frac{1}{2}$, results in a similar semiquantitative bound as in Eq. (1.3). Alternatively, one may define the perturbative boundary directly in terms of the Yukawa couplings; e.g., if we require the $\bar{t}bH$ coupling to be smaller than the QCD coupling $g_s^2 = 4\pi\alpha_s(M_W^2) \simeq 1.5$ we obtain the result

$$\tan\beta \gtrsim \frac{m_t}{600\ \text{GeV}} \tag{1.5}$$

as the definition of the perturbative region. We will use the constraint (1.5) in our following analysis. The above bounds apply equally to models I–IV. In models II and III there are also corresponding upper limits on $\tan\beta$, arising from the $\bar{t}bH$ coupling proportional to $m_b V_{tb} \tan\beta$; these limits are obtained from the above equations by replacing $m_t \to m_b$ and $\tan\beta \to \cot\beta$, and give $\tan\beta \lesssim 100$–200. Perturbative limits can also be obtained from an examination of the one-loop heavy-fermion corrections to the ZH^+H^- vertex and result[29] in quantitatively similar bounds to those of Eqs. (1.3) and (1.5).

II. CONSTRAINTS FROM LOW-ENERGY DATA

In this section we first review the analytical calculations for each process that we consider and present the results from our combined analysis at the end.

A. Neutral meson mixing

1. B^0-$\bar{B}^0$ mixing

It has been shown[7] that charged Higgs bosons can give sizable contributions to B_d^0-$\bar{B}_d^0$ mixing and can account for the observed[30] value of this mixing at ARGUS and CLEO without requiring the top quark to be heavy. B_d^0-$\bar{B}_d^0$ mixing proceeds through the box diagrams shown in Fig. 2 (with $q = b$), where contributions due to W, H, and ϕ (ϕ being the unphysical Higgs field in the SM) exchange are all included. The B_L-B_S mass difference is (in model II)

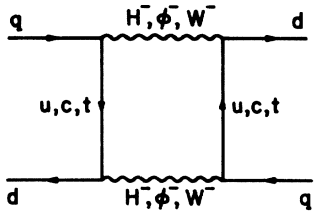

FIG. 2. Box diagrams contributing to neutral meson antimeson mixing.

$$\Delta M_B = 2|M_{12}| = \frac{G_F^2 M_W^2}{6\pi^2} m_B f_B^2 B_B |(V_{tb}V_{td}^*)^2| \eta_t \times [A_{WW}(x_t) + \cot^4\beta A_{HH}(x_t,x_H,x_b) + \cot^2\beta A_{WH}(x_t,x_H,x_b)] , \quad (2.1)$$

where $x_i = m_i^2/M_W^2$, η_t is a QCD correction factor,[31] $A_{WW}(x_t)$ is given by the SM (Ref. 32), and the expressions for the functions A are given in Appendix A. For completeness we have included the contributions to A_{HH} and A_{WH} that arise from the $m_b\tan\beta$ term in the $\bar{t}bH$ coupling. This extra coupling results in a term which is of relative size $(m_b/m_t)\tan^2\beta$ and can give significant effects when $\tan\beta$ is large, i.e., for $\tan\beta \gtrsim 5$ it can compete with the $m_t\cot\beta$ contribution. In contrast, the contributions from the external momentum of the b quark are proportional to m_b/m_t and are approximately the same size as they are in the SM (of order[33] 5–10%) and hence we neglect the b-quark external momentum here. The dominance of the t quark in the loops is assumed and in the limit of $m_b = 0$ our results agree with those of Glashow and Jenkins.[7] The corresponding expression for ΔM_B in model I is also given by Eq. (2.1) with $\tan\beta \to 1$ in the formulas for A_{HH} and A_{WH} given in Eqs. (A2) and (A3). Since the $H^\pm$ coupling proportional to $m_t\cot\beta$ generally dominates in Eq. (2.1) the limits on the charged Higgs parameters from B^0-$\bar{B}^0$ mixing do not differ between models I and II for values of $\tan\beta$ in the range 0.1–100. The relevant hadronic matrix elements contributing to Eq. (2.1) are

$$\langle \bar{B}^0|[\bar{d}\gamma^\lambda(1-\gamma_5)b][\bar{d}\gamma_\lambda(1-\gamma_5)b]|B^0\rangle = \frac{8}{3}\frac{f_B^2 B_B m_B^2}{2m_B} \quad (2.2)$$

and for the $m_b\tan\beta$ Higgs coupling term

$$\langle \bar{B}^0|[\bar{d}(1+\gamma_5)b][\bar{d}(1+\gamma_5)b]|B^0\rangle = \frac{\frac{8}{3}f_B^2 B_B \frac{m_B^4}{m_b^2}}{2m_B} \simeq \frac{\frac{8}{3}f_B^2 B_B m_B^2}{2m_B} , \quad (2.3)$$

where f_B is the B meson decay constant.

The QCD corrections to the charged-Higgs-boson contributions have not yet been calculated. However, it is reasonable to assume that these corrections are about the same as those for the W and unphysical-Higgs-boson exchange diagrams. We can in fact test the sensitivity to this choice by comparing the case where the corrections are included in A_{WH} and A_{HH} with the case where they are not. We find that in both cases our resulting constraints on $m_{H^\pm}$ and $\tan\beta$ are basically the same. We include the QCD corrections in all contributions to Eq. (2.1).

In our numerical evaluations we take $n_t = 0.85$, $m_B = 5.275$ GeV, $M_W = 80.0$ GeV, $m_b = 5$ GeV, $\tau_B = (1.15 \pm 0.14)$ ps (Ref. 30), and following Ref. 34 we let $f_B B_B^{1/2}$ lie in the range $100 \le f_B B_B^{1/2} \le 180$ MeV. Recent lattice computations[35] find values for $f_B B_B^{1/2}$ of 105 ± 35 MeV (Bernard *et al.*), 130 ± 20 MeV (Hamber), and ~ 120 MeV (Gavela *et al.*), which are consistent with our range. The combined ARGUS and CLEO data[30] measure the ratio of like-sign to unlike-sign dileptons from $\Upsilon(4S) \to B_d^0 \bar{B}_d^0$ states which gives the result $x_{B_d} = 0.70 \pm 0.13$, where $x_{B_d} = \Delta M_B/\Gamma_{B_d}$.

In the case of the SM, t-quark contributions also dominate B_s^0-$\bar{B}_s^0$ mixing. The ratio $R = x_{B_s}/x_{B_d}$ is then roughly given by

$$R \simeq \frac{|V_{ts}|^2}{|V_{td}|^2} \gg 1 \quad (2.4)$$

due to the hierarchial structure of the KM matrix; hence B_s^0-$\bar{B}_s^0$ mixing is constrained to be maximal in the SM. This result also holds in two-Higgs-doublet models since t-quark dominance persists in the $H^\pm$ contributions and, as can be seen from Eq. (2.1), the same KM factors are involved in both the SM and $H^\pm$ terms. Thus R has roughly the same value in the presence of $H^\pm$ bosons as it does in the SM.

2. D^0-$\bar{D}^0$ mixing

D^0-$\bar{D}^0$ mixing is also mediated by the Feynman diagrams presented in Fig. 2 with $q = c$, $d \to u$, and $c, t \to s, b$. The experimental upper limit[36,37] on the D mass difference is $\Delta M_D < 1.3 \times 10^{-13}$ GeV. The SM box-diagram contributions, in which the b quark is dominant and the external momentum terms (proportional to m_c/m_b) are no longer negligible, are quite small[38] giving $\Delta M_D \approx 10^{-17}$. However, the long-distance contributions, consisting of $\pi\pi$ and KK intermediate states, are estimated[39] to be larger giving $\Delta M_D \sim 0.7$–30×10^{-15}. We find that the charged-Higgs-boson contributions can also be significant, and demand that these $H^\pm$ contributions alone not exceed the experimental bound on ΔM_D.

Including the terms arising from the charged Higgs couplings to the masses of the external quarks (i.e., $m_c\cot\beta$), the $H^\pm$ box-diagram contributions to ΔM_D are (in model II, taking $m_s = 0$)

$$\Delta M_D = \frac{G_F^2 M_W^2}{6\pi^2} m_D f_D^2 B_D |(V_{cb}^* V_{ub})^2| \times [\tan^4\beta A_{HH}(x_b, x_H, x_c) + \tan^2\beta A_{WH}(x_b, x_H, x_c)] , \quad (2.5)$$

where the explicit expressions for A_{HH} and A_{WH} can again be found in Appendix A with the substitution $\tan\beta \to \cot\beta$ in Eqs. (A2) and (A3). The dominant contribution in Eq. (2.5) involves the Higgs-fermion coupling proportional to m_b and hence D^0-$\bar{D}^0$ mixing does differentiate between models I and II. The expression for ΔM_D in model I is given by the substitution $\tan\beta \to \cot\beta$ in Eq. (2.5) and $\tan\beta \to 1$ in Eqs. (A2) and (A3). As discussed below, we find that D-meson mixing only constrains the charged Higgs sector in the case of model II (and then only for very large $\tan\beta$, i.e., $\tan\beta \gtrsim$ few $\times 10^2$, which is beyond the perturbative limit); there are no additional restrictions in model I after the constraints from B^0-$\bar{B}^0$ mixing are taken into account. Numerically, we set $m_D = 1.87$ GeV, $m_c = 1.5$ GeV, $\tau_D = 4.28 \times 10^{-13}$ s, and consider $f_D B_D^{1/2}$ to lie[34] in the range 170 ± 50 MeV. Note that the value $f_D B_D^{1/2} = 120$ MeV gives the most conservative limits from Eq. (2.5) and hence is the value we use in our calculations.

3. K^0-$\bar{K}^0$ mixing

We consider the influence of charged Higgs bosons on the K_L-K_S mass difference. These contributions are again represented by the box diagrams in Fig. 2 with $q = s$. The short-distance contributions to ΔM_K are directly related to the B_L-B_S mass difference via (in both models I and II assuming $m_s = 0$)

$$\Delta M_K = \left| \frac{(V_{ts} V_{td}^*)^2}{(V_{tb} V_{td}^*)^2} \right| \frac{f_K^2 m_K}{f_B^2 m_B} \Delta M_B \quad (2.6)$$

with $f_K = 160$ MeV and $m_K = 0.497$ GeV. The SM calculation for ΔM_K is plagued by uncertainties[40] from long-distance effects, as well as short-distance strong-interaction corrections and evaluation of the hadronic matrix elements. However, the K_L-K_S mass difference has been widely used[41] to constrain new physics by demanding that the new physics contributions not exceed the experimental determination of ΔM_K. We thus require that (with ΔM_K as calculated above)

$$|\Delta M_K| \leq (\Delta M_K)_{\text{expt}} \pm (3.521 \pm 0.014) \times 10^{-15} \text{ GeV} . \quad (2.7)$$

A recent calculation[40] in the large-N approach yields the more stringent restriction

$$|\Delta M_K(\text{new physics})| \leq 0.1 (\Delta M_K)_{\text{expt}} ; \quad (2.8)$$

however, we make use of the weaker bound (2.7).

B. *CP* violation

1. ϵ parameter

As is well known, the parameter ϵ is a measure of *CP* violation in the physical states of the K^0-$\bar{K}^0$ system. The general expression for ϵ is given by the imaginary part of the off-diagonal matrix element ($\text{Im}M_{12}$) of the $\Delta S = 2$ effective Hamiltonian as[33,42]

$$\epsilon \simeq \frac{e^{i\pi/4}}{\sqrt{2}\Delta M_K} \text{Im} M_{12} \quad (2.9)$$

in the reasonable approximation that the imaginary part of the $\Delta I = \frac{1}{2}$ transition amplitude is neglected in comparison to its real part, and where M_{12} is given by the off-diagonal element of the $K^0, \bar{K}^0$ mass matrix. The charged-Higgs-boson contributions to M_{12} arise from the Feynman diagrams displayed in Fig. 2 with $q = s$. The resulting expression for ϵ is (in both models I and II with $m_s = 0$)

$$\epsilon = \frac{e^{i\pi/4}}{\sqrt{2}\Delta M_K} \frac{G_F^2 M_W^2}{12\pi^2} m_K f_K^2 B_K \text{Im}\{\eta_{cc}\lambda_c^2 A_{WW}(x_c) + \eta_{tt}\lambda_t^2 A_{WW}(x_t) + 2\eta_{ct}\lambda_c\lambda_t A_{WW}^{ct}(x_c, x_t) + \cot^4\beta[\eta_{cc}\lambda_c^2 A_{HH}(x_c, x_H, x_s = 0) + \eta_{tt}\lambda_t^2 A_{HH}(x_t, x_H, x_s = 0) + 2\eta_{ct}\lambda_c\lambda_t A_{HH}^{ct}(x_c, x_t, x_H)] + \cot^2\beta[\eta_{cc}\lambda_c^2 A_{WH}(x_c, x_H, x_s = 0) + \eta_{tt}\lambda_t^2 A_{WH}(x_t, x_H, x_s = 0) + 2\eta_{ct}\lambda_c\lambda_t A_{WH}^{ct}(x_c, x_t, x_H)]\} , \quad (2.10)$$

where the functions A are given in Appendix A, η_{ij} are the QCD corrections, and $\lambda_i = V_{is} V_{id}^*$. We take[31] the η values $\eta_{cc} = 0.70$, $\eta_{ct} = 0.40$, $\eta_{tt} = 0.65$. The experimental value[37] of ϵ is $(2.259 \pm 0.018) \times 10^{-3} e^{i\pi/4}$. The major uncertainty lies in the value of the bag factor B_K, which is the ratio of hadronic matrix elements ($B_K = 1.0$ in the vacuum-saturation approximation). Estimates[43] of B_K vary widely, ranging from -0.4 to 2.9. Recent lattice computations[35] yield $B_K \simeq 0.5$–1.2 and we allow B_K to vary in the most probable range $\frac{1}{3}$–1.5.

2. ϵ' parameter

A second parameter, ϵ', describes the source of direct *CP* violation in the decay $K^0 \to 2\pi$. Defining $\langle \pi\pi(I = n)|H_W|K^0\rangle \equiv A_n e^{i\delta_n}$, where δ_n is the phase

shift in the $\pi\pi(I=n)$ final state, ϵ' is given by

$$\epsilon'=\frac{e^{i(\delta_2-\delta_0+\pi/2)}}{\sqrt{2}}\frac{\mathrm{Re}A_2}{\mathrm{Re}A_0}\left[\frac{\mathrm{Im}A_2}{\mathrm{Re}A_2}-\frac{\mathrm{Im}A_0}{\mathrm{Re}A_0}\right]. \tag{2.11}$$

Some of these parameters have been experimentally determined,[37,44] giving $\delta_2-\delta_0+\pi/2=(48\pm8)^\circ\simeq\pi/4$, $\mathrm{Re}A_2/\mathrm{Re}A_0=0.05$, $|A_0|=2.71\times10^{-7}$ GeV. The leading contribution to the imaginary parts of the $K^0\to2\pi$ $\Delta S=1$ amplitude is given by the gluon-exchange penguin diagram depicted in Fig. 3(a) with $q=s$, $q'=d$, and f represents a $\bar{d}$ quark. The gluon-exchange penguin only contributes to the $\Delta I=\frac{1}{2}$ amplitude (A_0), while the electromagnetic penguin diagram (γ exchange) contributes to both A_0 and A_2 but is suppressed by a factor of order α/α_s. We thus presently ignore the electromagnetic penguin contributions, but will briefly discuss their relative importance later.

The general $\bar{d}sg$ vertex takes the form

$$ig_s\bar{d}\Gamma_\mu s g^\mu, \tag{2.12}$$

where Γ_μ is decomposed as

$$\Gamma_\mu=F_1\gamma_\mu(1-\gamma_5)+F_2q_\mu(1+\gamma_5)+F_3\sigma_{\mu\nu}q^\nu(1+\gamma_5). \tag{2.13}$$

The q^2 term of the $F_1\gamma_\mu(1-\gamma_5)$ piece is the dominant contribution since the gluon is attached to a massless quark and the F_3 term scales like an additional factor of m_s^2/M_W^2. The effective $\Delta S=1$ weak Hamiltonian is given by[33,34]

$$H_{\mathrm{eff}}=\frac{G_F}{\sqrt{2}}\frac{\alpha_s}{12\pi}\sum_i\lambda_iF_W(x_i)Q_6$$
$$=\frac{G_F}{\sqrt{2}}\sum_i\lambda_i\frac{\alpha_s}{12\pi}[\ln(x_i)-H(x_i)]Q_6 \tag{2.14}$$

with $\lambda_i=V_{id}V_{is}^*$. $F_W(x_i)$ is furnished in Appendix A, and the operator Q_6 is defined by

$$Q_6=\bar{d}\gamma_\mu\lambda^q(1-\gamma_5)s(\bar{u}\gamma^\mu\lambda_a u+\bar{d}\gamma^\mu\lambda_a d+\bar{s}\gamma^\mu\lambda_a s). \tag{2.15}$$

In the SM we then have

$$\xi\equiv\frac{\mathrm{Im}A_0}{\mathrm{Re}A_0}=\frac{-G_F}{\sqrt{2}}\frac{\langle\pi\pi(I=0)|Q_6|K^0\rangle}{2.71\times10^{-7}\ \mathrm{GeV}}(\mathrm{Im}\lambda_t)C_I. \tag{2.16}$$

Here C_I is defined[34] to be

$$C_I=C_I^{\mathrm{GP}}\frac{F_W(x_t)}{\ln(m_t^2/m_c^2)}, \tag{2.17}$$

where C_I^{GP} is the resummation of leading logarithms [i.e., the resummation of $(\alpha_s/12\pi)\ln(x_i)$] by Guberina and Peccei.[45] C_I is evaluated[34] to be 0.088 ± 0.042 for m_t in the range 40–200 GeV (it is rather insensitive to m_t), for the QCD scale $\Lambda=100$–200 MeV, and with μ^2 (the scale at which the matrix elements are evaluated) between 0.5 and 1 GeV. An estimation[46] of the matrix element based on vacuum saturation and current algebra gives

$$\langle\pi\pi(I=0)|Q_6|K^0\rangle$$
$$\simeq\frac{16}{9}\frac{f_\pi m_K^2 m_\pi^2}{m_s(m_u+m_d)}\left[\frac{f_K}{f_\pi}-1+\frac{f_K}{f_\pi}\frac{m_K^2}{m_\sigma^2}\right] \tag{2.18}$$

which yields $\langle\pi\pi(I=0)|Q_6|K^0\rangle\simeq0.2$–$0.8$ when the following values[47] of masses (evaluated at a scale $\mu=1$ GeV),

$$m_u=(5.1\pm1.5)\ \mathrm{MeV},\quad m_d=(8.9\pm2.6)\ \mathrm{MeV},$$
$$m_s=(175\pm55.0)\ \mathrm{MeV},\quad m_\sigma=(0.7\text{–}0.9)\ \mathrm{GeV}, \tag{2.19}$$

are used.

The charged-Higgs-boson contributions to the $\bar{d}sg$ vertex are shown in Figs. 3(b) (i)–3(b) (iii). Since the operator structure of the $H^\pm$ contribution is the same as that for the SM, the resulting expression for ϵ' including SM and $H^\pm$ contributions is simply (in both models I and II with $m_s=0$)

$$\epsilon'=\frac{e^{i\pi/4}}{\sqrt{2}}\frac{\mathrm{Re}A_2}{\mathrm{Re}A_0}\xi\left[1+\cot^2\beta\frac{F_H(y_t)-F_H(y_c)}{F_W(x_t)-F_W(x_c)}\right] \tag{2.20}$$

with $y_i=m_i^2/m_{H^\pm}^2$. $F_H(y)$ is presented in Appendix A and can be easily obtained from the general formulas for the charged-Higgs-boson contributions to the $\bar{q}'qG$ (G being a γ, Z, or gluon) vertex presented in Ref. 14. As a

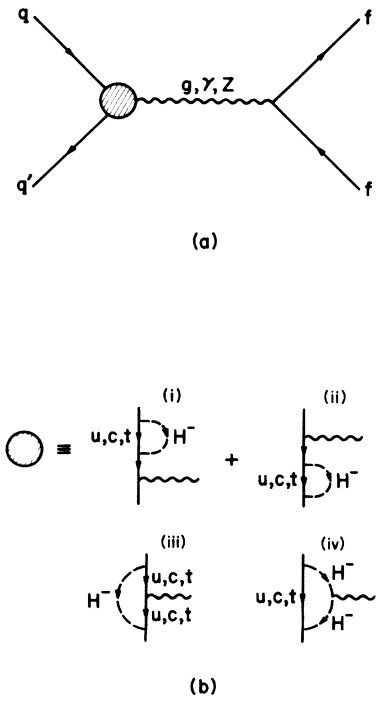

FIG. 3. Penguin diagrams contributing to meson decays and ϵ'/ϵ: (a) overall structure showing gluon, photon, Z exchanges; (b) charged-Higgs-boson contributions to the $\bar{q}'qG$ vertex ($G=g,\gamma,Z$).

check on the form of $F_H(y)$, we note that in the limit of $m_t \to 0$, the ratio of charged-Higgs-boson to W-boson penguin contributions reproduces the result of Athanasiu and Gilman,[8] i.e., for $m_c^2 \ll m_t^2 \ll M_W^2$,

$$\frac{\cot^2\beta[F_H(y_t)-F_H(y_c)]}{F_W(x_t)-F_W(x_c)} \to \frac{1}{2}\cot^2\beta \frac{y_t \ln y_t}{\ln(m_t^2/m_c^2)} . \quad (2.21)$$

The experimental value of ϵ'/ϵ is in a state of flux with the two recent and somewhat contradictory results

$$\begin{aligned} &\text{NA31 at CERN}^{48} \quad \epsilon'/\epsilon=(3.3\pm1.1)\times10^{-3} , \\ &\text{E731 at Fermilab}^{49} \quad \epsilon'/\epsilon=(-5\pm14\pm6)\times10^{-4} . \end{aligned} \quad (2.22)$$

In setting restrictions on $m_{H^\pm}$ and $\tan\beta$ from our combined analysis we first conservatively assume that $|\epsilon'/\epsilon| \le 5\times10^{-3}$, and we find that this limit has no significant effect on our bounds. After all of our constraints are combined, we then restrict ϵ'/ϵ to lie within the $\pm2\sigma$ range of the published NA31 data and obtain further constraints on two-doublet models.

Defining R to be the quantity in large parentheses in Eq. (2.20), i.e., $R \equiv \{1+\cot^2\beta[F_H(y_t)-F_H(y_c)]/[F_W(x_t)-F_W(x_c)]\}$, ϵ'/ϵ is given by

$$\frac{\epsilon'}{\epsilon} = \left[\frac{\epsilon'}{\epsilon}\right]_{\rm SM} \left[\frac{\xi}{\xi_{\rm SM}}\right] R . \quad (2.23)$$

Deviations of R from unity are due to the effects of the charged-Higgs-boson contributions. In the SM the expected value of ϵ'/ϵ lies in the approximate range[33,34,42] $10^{-3} \lesssim \epsilon'/\epsilon \lesssim 10^{-2}$. In Fig. 4 we display R as a function of $\tan\beta$ for various values of m_t and $m_{H^\pm}$. Clearly, for smaller values of $\tan\beta$ and $m_{H^\pm}$ (e.g., $\tan\beta \lesssim 0.2$ and $m_{H^\pm} \lesssim 100$ GeV) the $H^\pm$ penguin contributions are large and negative. For some values of the parameters (namely, $\tan\beta \lesssim 0.3$ and $m_{H^\pm} \lesssim 250$ GeV), the predicted value of ϵ'/ϵ is found to be quite small and negative and can be consistent with the preliminary Fermilab E731 data. For other values of the parameters $R \approx 1$ (namely, for $\tan\beta \gtrsim 0.4$) and ϵ'/ϵ is found to agree with the data of the NA31 experiment at CERN.

It has recently been emphasized[50] that the electromagnetic penguin (i.e., γ and Z exchange) contributions to ϵ'/ϵ may be significant (especially if the top quark is heavy), having the effect of reducing the predicted value of ϵ'/ϵ. Presumably, the $H^\pm$ contributions to the electromagnetic penguin diagrams may also be large (these

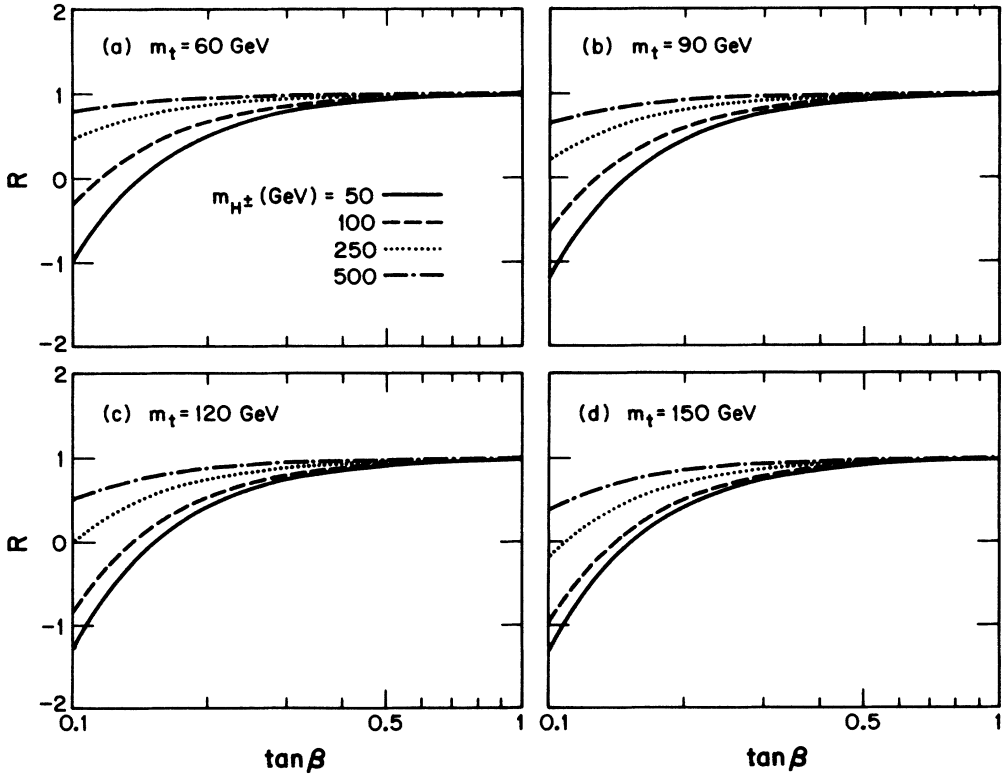

FIG. 4. The factor R defined in Eqs. (2.20)–(2.23), describing the correction to the SM value of ϵ'/ϵ due to $H^\pm$ contributions, is shown vs $\tan\beta$ for (a) $m_t = 60$ GeV, (b) $m_t = 90$ GeV, (c) $m_t = 120$ GeV, (d) $m_t = 150$ GeV. The results are the same for both models I and II. Solid, dashed, dotted, dashed-dotted curves denote the cases $m_{H^\pm} = 50$, 100, 250, and 500 GeV, respectively.

diagrams are easily calculable from the general expressions contained in Ref. 14). However, the calculations of the matrix elements for the appropriate operators are even more uncertain[46,50] in this case than for the gluonic penguin, and thus we ignore electromagnetic penguin effects in our analysis.

The influence of charged Higgs bosons on the electric dipole moment of the neutron (d_n) has been recently considered,[51] where it was found that the predicted value of d_n in two-doublet models is approximately the same as in the SM ($d_n \approx 10^{-32\pm1}$). Given the present gap[51] between experimental limits ($d_n \lesssim 10^{-25}$) and the SM prediction for d_n, it is impossible to restrict the parameters in two-doublet models from these considerations.

C. $B \to K^* \gamma$

Radiative B decays[52] proceed through the inclusive quark-level dipole transition $b \to s\gamma$ via the generic Feynman diagram displayed in Fig. 3(a) with $q = b$, $q' = s$, and the γ is taken on-shell. The diagrams responsible for the charged-Higgs-boson contributions to $b \to s\gamma$ with an on-shell γ are shown in Figs. 3(b) (iii) and 3(b) (iv). The matrix element for this process is governed by the $F_3 \sigma_{\mu\nu} q^\nu (1+\gamma_5)$ term in Eq. (2.13) and results in the decay rate

$$\Gamma(b \to s\gamma) = \frac{\alpha G_F^2 m_b^5}{128\pi^4} \left| \sum_{i=c,t} \lambda_i [G_W(x_i) + a G_H^1(y_i) + \cot^2\beta G_H^2(y_i)] \right|^2 . \quad (2.24)$$

Here, $\lambda_i = V_{is}^* V_{ib}$, $a = -\cot^2\beta$ in model I, $a = +1$ in model II, and $G_W, G_H^{1,2}$ can be found in Appendix A. G_W represents the SM contribution[32] and $G_H^{1,2}$ is the $H^\pm$ contribution given in Refs. 11 and 14. This process differentiates model I from model II and we will see that the predicted branching ratio is quite different in the two cases. The branching ratio is given by

$$B(b \to s\gamma) = \frac{\Gamma(b \to s\gamma)}{\Gamma(b \to ce\bar{\nu})} B(b \to ce\bar{\nu}) . \quad (2.25)$$

It has been shown[53] that the QCD radiative corrections significantly enhance the rate for $b \to s\gamma$, since they have the effect of replacing the m_t^2/M_W^2 GIM power suppression in G_W with a m_t^2/M_W^2 logarithmic suppression. As pointed out in Grinstein and Wise[11] the QCD corrections are applied to the dipole transition operator of the matrix element and hence all contributions to this operator (in this case from the SM and $H^\pm$) receive the same QCD radiative corrections. We employ the prescription of Grinstein, Springer, and Wise[53] for these corrections to

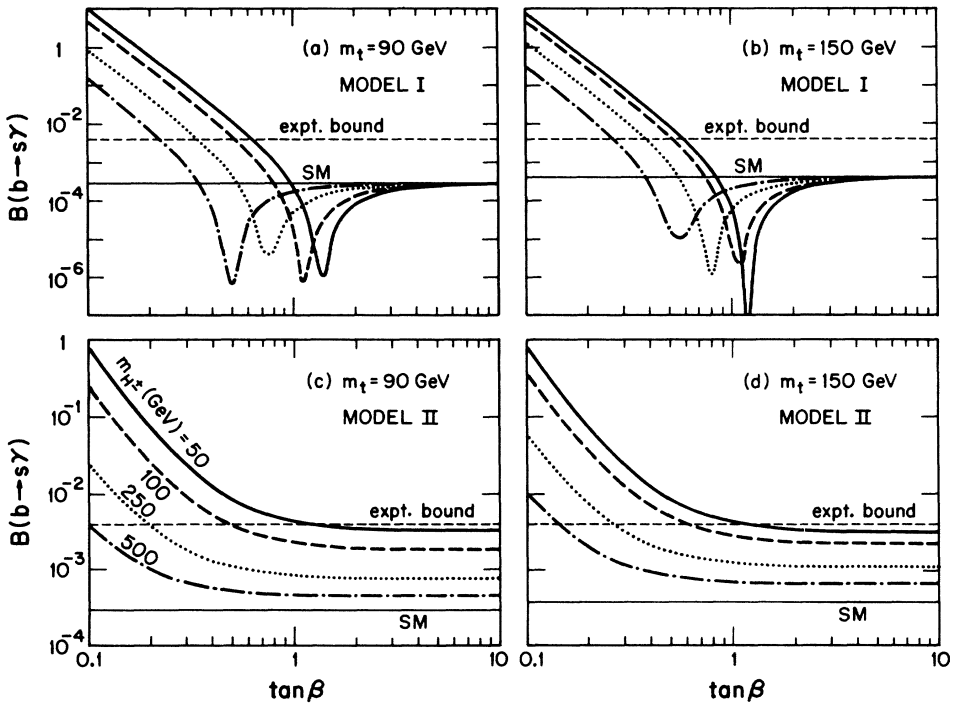

FIG. 5. The branching fraction for the decay $b \to s\gamma$ is shown vs $\tan\beta$ for various $m_{H^\pm}$ values, in (a) model I with $m_t = 90$ GeV, (b) model I with $m_t = 150$ GeV, (c) model II with $m_t = 90$ GeV, (d) model II with $m_t = 150$ GeV. Solid, dashed, dotted, dashed-dotted curves correspond to $m_{H^\pm} = 50$, 100, 250, and 500 GeV, respectively.

$$c_7(M_W)=G_W(x_i)+aG_H^1(y_i)+\cot^2\beta G_H^2(y_i)\ , \quad (2.26)$$

with the result

$$c_7(m_b)=[\alpha_s(M_W)/\alpha_s(m_b)]^{16/23} \times\left[c_7(M_W)-\frac{3x}{10}\{[\alpha_s(m_b)/\alpha_s(M_W)]^{10/23}-1\} -\frac{3x}{28}\{[\alpha_s(m_b)/\alpha_s(M_W)]^{28/23}-1\}\right], \quad (2.27)$$

where $x=232/81$.

Experimentally one must search for an exclusive mode, typically $B\to K^*\gamma$, where the current limit[54] is $B(B\to K^*\gamma)<2.4\times10^{-4}$. The ratio of exclusive to inclusive rates contains great theoretical uncertainty, making comparisons of theory to experiment difficult. A recent (and conservative) estimate[55] is $\Gamma(B\to K^*\gamma)/\Gamma(b\to s\gamma)=0.06$, which when combined with the data on the exclusive branching fraction yields the inferred bound $B(b\to s\gamma)<4\times10^{-3}$. We will see that this level of sensitivity is beginning to confront the possible branching fraction enhancements due to $H^\pm$ contributions, and that any future increase in experimental sensitivity will either further restrict the parameters in the charged Higgs sector or reveal new physics.

Figure 5 shows $B(b\to s\gamma)$ including SM and $H^\pm$ contributions as a function of $\tan\beta$ in both models I and II with $m_t=90,150$ GeV and for various values of $m_{H^\pm}$. For comparison, the SM branching fraction and the inferred experimental upper bound are also depicted in the figure. We have performed our own fit of the SM results in terms of m_t and find that the branching fraction is roughly given by

$$B(b\to s\gamma)\simeq 2.91\times10^{-4}\left[\frac{m_t}{90\text{ GeV}}\right]^{0.53}. \quad (2.28)$$

It is clear from Fig. 5 that especially large enhancements or suppressions of the branching fraction are possible in model I. This is due to the fact that $a=-\cot^2\beta$ in model I and can thus cause destructive interference with the SM contributions. This destructive interference between the SM and $H^\pm$ terms does not occur in model II, where the charged-Higgs-boson contributions are found to always enhance the SM rate. Note that for some values of the parameters (namely, $\tan\beta\gtrsim 1$ for $m_{H^\pm}\lesssim 100$ GeV) the total branching fraction already exceeds the present experimental limit.

D. $K_L\to\mu\mu$

Interest in the process $K_L\to\mu\mu$ has been revived due to two new measurements[56] of its branching fraction of $B(K_L\to\mu\mu)=(8.4\pm1.1)\times10^{-9}$ and $B(K_L\to\mu\mu)=(5.8\pm0.72)\times10^{-9}$, which are lower than the previous[37] world average of $B=(9.58^{+2.4}_{-1.5})\times10^{-9}$. It is well known that the intermediate 2γ state dominates the imaginary part of the amplitude for this process and calculations[57] yield $B(K_L\to2\gamma\to\mu\mu)=(6.83\pm0.28)\times10^{-9}$. Geng and Ng[57] have averaged these two recent measurements of $B(K_L\to\mu\mu)$ with the previous value, and then subtracted the 2γ contribution to obtain a constraint on the real part of the amplitude of $B[\mathrm{Re}A(K_L\to\mu\mu)]<1.5\times10^{-9}$. If no cancellations occur between the short- and long-distance contributions to the real part of this amplitude then the short-distance contributions alone obey this constraint. However it has been shown in Ref. 58 that such cancellations may in fact occur and thus no restrictions on the short-distance contributions may be obtained from this process. In any case we find that the above constraint of Ref. 57 on the short-distance contributions to $K_L\to\mu\mu$ provides no additional constraints on $m_{H^\pm}$ and $\tan\beta$ once the bounds from ϵ have been taken into account.

The diagrams that may potentially contribute to the real part of the SM and $H^\pm$ short-distance amplitude for $K_L\to\mu\mu$ are shown in Fig. 2 (with $q=s$ and a muon line replacing the quark line on the right) and Fig. 3 (with $q=s$, $q'=d$, $f=\mu$, and a Z boson is exchanged). Note that for on-shell muons in the final state, electromagnetic current conservation leads to a null contribution from the photon-exchange term. The weak interaction contribution to the decay width is (in models I and II with $m_s=0$)

$$\Gamma(K_L\to\mu\mu)=\frac{G_F^4M_W^4}{64\pi^5}f_K^2m_\mu^2m_K\left[1-\frac{4m_\mu^2}{m_K^2}\right]^{1/2} \times\left|\mathrm{Re}\lambda_tC_W(x_t)\left[1+\frac{C_H(y_t)}{C_W(x_t)}\right]^2\right|^2 \quad (2.29)$$

with $\lambda_t=V_{is}^*V_{id}$, C_W and C_H are given in Appendix A. We have calculated C_H from the results given in Ref. 14 for the $H^\pm$ contributions to $B\to\mu\mu$. The box diagrams with HH, HW, and $H\phi$ exchange are all found to be chirally suppressed by a factor of m_μ/M_W and are thus numerically negligible.

The branching fraction for the SM and $H^\pm$ short-distance contributions are presented in Fig. 6 as a function of $\tan\beta$ for several values of m_t and $m_{H^\pm}$, where we have assumed top-quark dominance and the value $|\lambda_t|=|(0.043)(0.005)|$ in our numerical calculations. The SM branching ratio is also shown. We see that the $H^\pm$ contributions can again give rise to large enhancements or suppressions over the SM rates.

E. $K^+\to\pi^+\nu\bar\nu$

The decay $K^+\to\pi^+\nu\bar\nu$ is mediated by the standard box and penguin-type diagrams of Figs. 2 and 3. In Fig. 2 $q=s$ on the left-hand side of the box and on the right-hand side, q and d are replaced by ν and $\bar\nu$ and the leptons e, μ, and τ are exchanged instead of u, c, and t. In the penguin graph of Fig. 3(a), $q=s$, $q'=d$, $f=\nu$, and a Z boson is exchanged. The charged-Higgs-boson contributions are shown in Figs. 3(b) (i)–(3b) (iv). The branching ratio for $K^+\to\pi^+\nu\bar\nu$ is then given by (in models I and II with $m_s=0$)

$$B(K^+\to\pi^+\nu\bar{\nu})=\frac{G_F M_W^2}{2\pi}\frac{B(K^+\to\pi^0 e^+\nu)}{|V_{us}|^2}\times\sum_{i=e,\mu,\tau}\left|\sum_{j=c,t}\lambda_j D(x_j^\alpha,z_i^\alpha)\right|^2, \quad (2.30)$$

where $\lambda_j=V_{js}^* V_{jd}$ and $D(x_j^\alpha,z_i^\alpha)$ is defined by

$$D(x_j^\alpha,z_i^\alpha)=D_{\rm SM}(x_j^\alpha,z_i^\alpha)+D_{WH}(x_j^\alpha,z_i^\alpha)+D_{HH}(x_j^\alpha,z_i^\alpha)+\cot^2\beta D_{ZH}(x_j^\alpha,z_i^\alpha), \quad (2.31)$$

with

$$x_{q_j}^\alpha=\frac{m(q_j)^2}{M_\alpha^2},\quad z_{l_i}^\alpha=\frac{m(l_i)^2}{M_\alpha^2}\quad(\alpha=W,H^\pm) \quad (2.32)$$

as appropriate. The functions $D(x_{q_j}^\alpha,z_{l_i}^\alpha)$ are given in Appendix A; $D_{\rm SM}$ (the SM box and penguin-diagram contributions) was calculated by Inami and Lim,[32] and D_{WH}, D_{HH}, and D_{ZH} (the contributions from the $WH^\pm$, and $H^\pm H^\pm$ exchange box diagrams, and $H^\pm$ penguin diagram, respectively) can be derived from the general formalism given in Ref. 14 and agree with the results presented in Refs. 10 and 15. D_{WH} and D_{HH} are proportional to the ratio $m_l^2/m_{H^\pm}^2$ and hence are numerically negligible. This process is also mediated by a single operator (due to the $V-A$ structure of the Z-boson neutrino coupling) and the QCD radiative corrections are again applied to this operator. We employ the QCD corrections calculated[59] for $D_{\rm SM}$ (which have been found to have a smaller effect than for $b\to s\gamma$) to $D=D_{\rm SM}+\cot^2\beta D_{ZH}$. The current experimental limit[60] on this branching ratio is $B(K^+\to\pi^+\nu\bar{\nu})<3.0\times10^{-8}$ and the BNL E-787 experiment expects to reach a sensitivity of $B(K^+\to\pi^+\nu\bar{\nu})\sim2\times10^{-10}$ in the future.

We incorporate the results of our combined analysis below in our calculations of $B(K^+\to\pi^+\nu\bar{\nu})$ (due to the dependency of the range of predicted branching fractions on the allowed values of the appropriate KM elements) and thus present our results for this branching fraction at the end of Sec. II F.

F. Combined analysis

Here we combine the results of the previous sections and determine the regions of charged-Higgs-boson parameter space which are consistent with low-energy data.

In the spirit of Ref. 61, a Monte Carlo analysis is employed in order to probe the freedom in the KM sector: 10^6 sets of the four parameters (3 mixing angles $\theta_{1,2,3}$ and 1 phase δ) present in the three-generation KM mixing

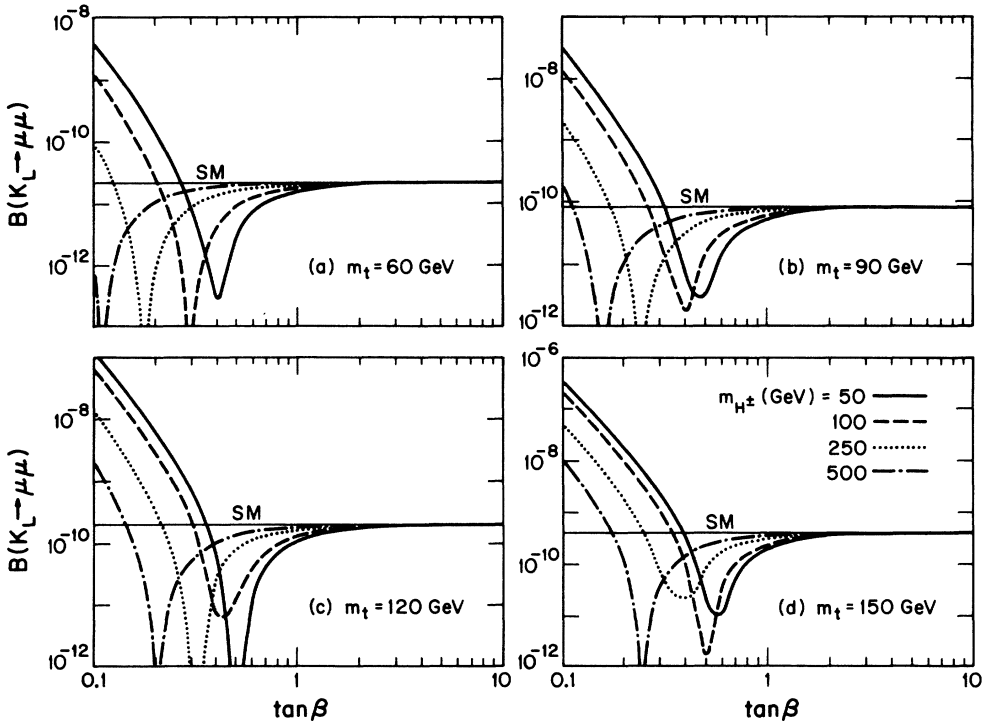

FIG. 6. The branching fraction for $K_L\to\mu\mu$ decay is shown vs tanβ for various $m_{H^\pm}$ values for (a) $m_t=60$ GeV, (b) $m_t=90$ GeV, (c) $m_t=120$ GeV, (d) $m_t=150$ GeV. The results are essentially the same for both models I and II. Solid, dashed, dotted, dashed-dotted curves represent the values $m_{H^\pm}=50$, 100, 250, and 500 GeV, respectively.

matrix are generated using the Kobayashi-Maskawa parametrization.[17] The parameters are generated subject to the restriction that the KM elements lie within their allowed ranges as determined in Ref. 37 from charged-current experiments and unitarity considerations. We find that 10^6 lotteries are sufficient to ensure that the parameter space is well sampled and converges at the boundaries of the allowed ranges for the KM elements. We also demand consistency (at the $\pm 2\sigma$ level) with the recent ARGUS and CLEO result[54] $|V_{ub}/V_{cb}| = 0.10 \pm 0.03$ obtained from the end-point spectrum of B semileptonic decays.

For each of the following values of m_t,

$$m_t = 60,\ 90,\ 120,\ 150 \text{ GeV} , \tag{2.33}$$

we vary $m_{H^\pm}$ and $\tan\beta$ in the ranges

$$m_{H^\pm} = 25\text{–}500 \text{ GeV},\quad \tan\beta = 0.1\text{–}10.0 , \tag{2.34}$$

and calculate B_d^0-$\bar{B}_d^0$ and D^0-$\bar{D}^0$ mixing, ϵ, ΔM_K, and ϵ'/ϵ, for each set of KM parameters which survive the above constraints on V_{ij}. In these calculations we explore the entire ranges of meson lifetimes, decay constants, and bag factors listed in Table II. We then demand that each of the above calculated quantities be consistent with the current experimental measurements discussed in the previous sections: i.e.,

$$\begin{aligned} &x_{B_d} = 0.70 \pm 0.13,\quad \Delta M_D < 1.3 \times 10^{-13} \text{ GeV} , \\ &\epsilon = (2.259 \pm 0.018) \times 10^{-3} , \\ &\Delta M_K = (3.521 \pm 0.014) \times 10^{-15} \text{ GeV} , \\ &|\epsilon'/\epsilon| < 5.0 \times 10^{-3} . \end{aligned} \tag{2.35}$$

We find that the data on B_d^0-$\bar{B}_d^0$ mixing and ϵ impose the strongest limits on the charged-Higgs-boson parameters $m_{H^\pm}$ and $\tan\beta$. Once the restrictions from ϵ have been satisfied, no additional constraints are obtained from considerations of ΔM_K or from requiring $|\epsilon'/\epsilon| < 5.0$

TABLE II. Values of the masses, lifetimes, decay constants, and bag factors used in our numerical calculations for the K^0, D^0, and B^0 mesons.

	m (GeV)	τ (ps)	f (MeV)	B
K	0.497		160	$\frac{1}{3}$–1.5
D	1.87	$(4.28 \pm 0.11) \times 10^{-1}$	170±50	1
B	5.275	1.15±0.14	140±40	1

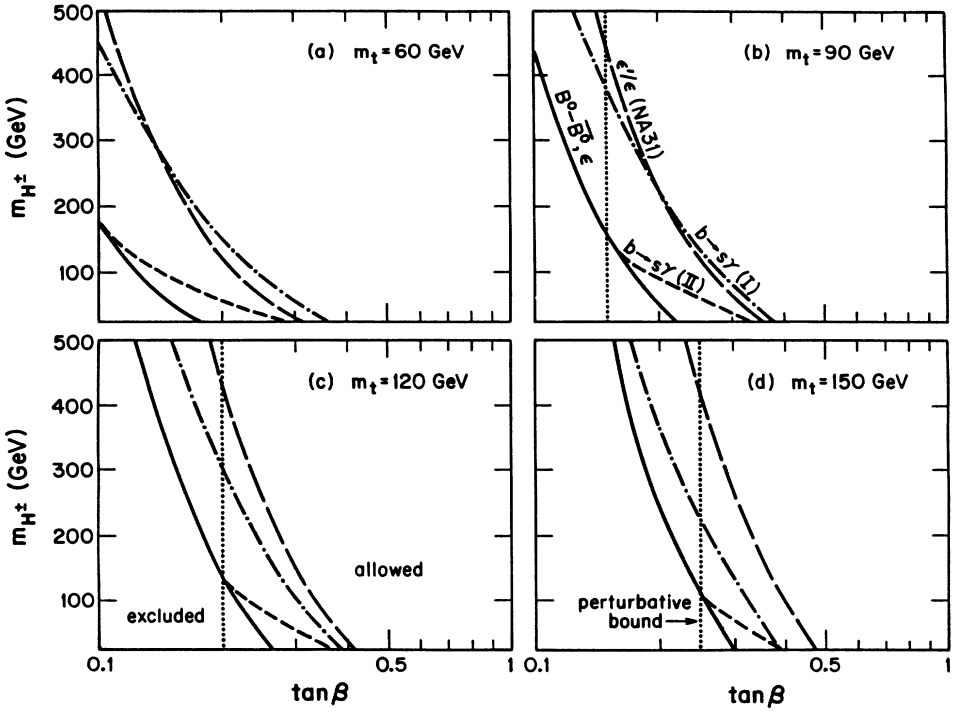

FIG. 7. Summary of restrictions from low-energy data on the charged-Higgs-boson mass $m_{H^\pm}$ and coupling parameter $\tan\beta$ for (a) $m_t = 60$ GeV, (b) $m_t = 90$ GeV, (c) $m_t = 120$ GeV, (d) $m_t = 150$ GeV. Regions to the left of the boundaries are excluded. The solid curve represents the combined constraints from B_d^0-$\bar{B}_d^0$ and D^0-$\bar{D}^0$ mixing, ΔM_K, ϵ, $|\epsilon'/\epsilon| < 5.0 \times 10^{-3}$, and $K_L \to \mu\mu$. The short-dashed, dashed-dotted, and long-dashed curves correspond to the constraints from $b \to s\gamma$ (model II), $b \to s\gamma$ (model I), and ϵ'/ϵ (NA31), respectively. The region excluded by perturbation theory is to the left of the dotted vertical line.

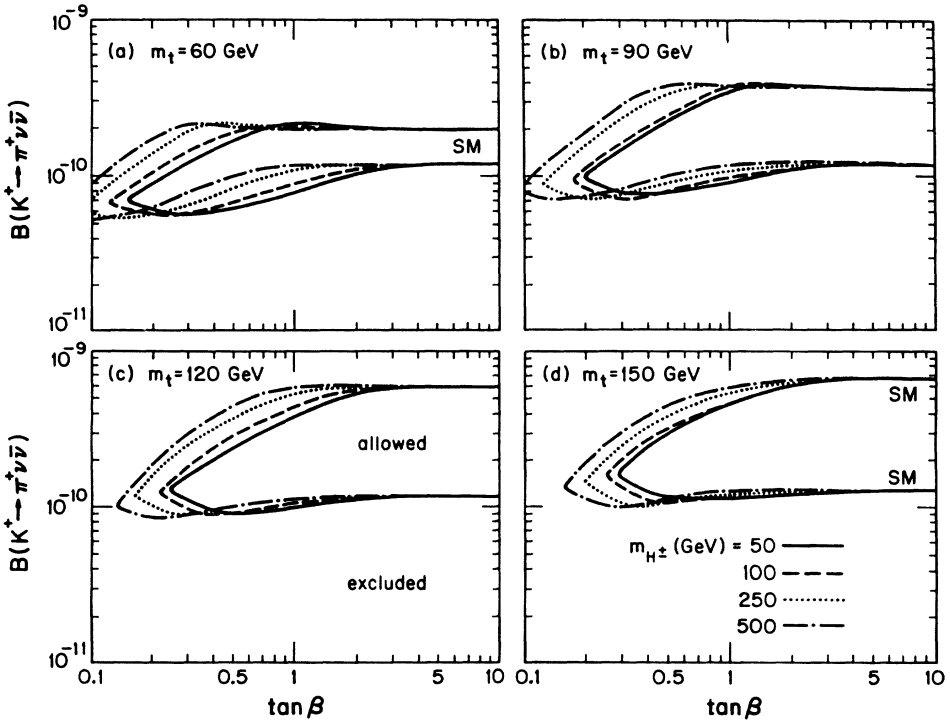

FIG. 8. The allowed regions for the branching fraction for $K^+ \to \pi^+ \nu\bar{\nu}$ decay are shown vs tanβ for various $m_{H^\pm}$ values with (a) $m_t = 60$ GeV, (b) $m_t = 90$ GeV, (c) $m_t = 120$ GeV, (d) $m_t = 150$ GeV for both models I and II. Solid, dashed, dotted, dashed-dotted curves denote the cases $m_{H^\pm} = 50$, 100, 250, and 500 GeV, respectively. The allowed regions lie between the curves. The results of Fig. 7 are imposed in the calculation of these branching fractions.

$\times 10^{-3}$. The possible constraints from the decay $K_L \to \mu\mu$ also do not reduce the allowed parameter space once the above restrictions are satisfied.

We then calculate $B(b \to s\gamma)$ in models I and II for the parameters which have survived all of the above constraints. Demanding consistency with the inferred experimental bound $B(b \to s\gamma) < 4.0 \times 10^{-3}$ we find additional limits on $m_{H^\pm}$ and tanβ in both models. Further bounds are also obtained by requiring ϵ'/ϵ to lie within $\pm 2\sigma$ of the published NA31 data of $\epsilon'/\epsilon = (3.3 \pm 1.1) \times 10^{-3}$.

The results from this analysis are presented in Fig. 7 which shows the allowed regions in the $m_{H^\pm}$,tanβ plane for $m_t = 60$, 90, 120, and 150 GeV. The solid curve corresponds to the combined restrictions from B_d^0-$\bar{B}_d^0$ and D^0-$\bar{D}^0$ mixing, ϵ, ΔM_K, and $|\epsilon'/\epsilon| < 5.0 \times 10^{-3}$, the short-dashed (dashed-dotted) curve depicts the constraints from the decay $b \to s\gamma$ in model II (I), the long-dashed curve represents the limits from the NA31 data on ϵ'/ϵ, and the dotted curve illustrates the perturbative bound of Eq. (1.5); for $m_t = 60$ GeV, the perturbative bound is tan$\beta \gtrsim 0.1$. The excluded regions lie to the left of the curves. Clearly, the constraints from these processes become stronger as the top quark becomes heavier. It is interesting to note that the perturbative bound alone provides a rough estimate of the combined restrictions for $m_{H^\pm} \gtrsim 100$ GeV (except for NA31 ϵ'/ϵ constraints).

In Fig. 8 we show the predicted values for the branching fraction for the decay $K^+ \to \pi^+ \nu\bar{\nu}$ as a function of tanβ with the values of m_t and $m_{H^\pm}$ as indicated. The allowed regions lie between the curves. The results of our above analysis [including the constraints of Eq. (2.35) only] are incorporated in our calculations for $B(K^+ \to \pi^+ \nu\bar{\nu})$. The SM predictions for this branching fraction coincide with these results at large tanβ (i.e., tan$\beta \gtrsim 3$). We see that for all values of $m_{H^\pm}$ and for tan$\beta \lesssim 3$ the charged-Higgs-boson contributions have the effect of narrowing and slightly suppressing the range of allowed branching fractions compared to the SM predictions. For tan$\beta \gtrsim 3$ the SM contributions become dominant.

III. CONSTRAINTS FROM $\bar{p}p$ COLLIDER DATA

A. Searches for top and large missing E_T

Heavy quarks can be produced at the CERN and Fermilab $\bar{p}p$ colliders at masses well beyond the range accessible to present e^+e^- machines. Top-quark signals (based on SM semileptonic decays $t \to b\bar{l}\nu$ with $l = e$ or μ) have been sought[16,62] but have not yet been found; this places lower limits on the mass m_t in the SM. But m_t values below these limits are possible, provided the SM decays are somehow sufficiently suppressed. In the present context of two-Higgs-doublet models, such

suppression can be provided by competition with nonstandard top decays via a real or virtual charged Higgs boson, $t \to bH^+$ (the eventual charged leptons from $H^+ \to \bar{\tau}\nu$, $\bar{\tau} \to \bar{l}\nu\bar{\nu}$ have a much softer spectrum than those from $t \to b\bar{l}\nu$ and few survive the experimental cuts). Hence for "SM excluded" values of m_t (i.e., for $m_t < 77$ GeV) the nonobservation of top signals may be used to constrain the parameters in the charged Higgs sector by requiring sufficient competition from $t \to bH^+$ modes. Loosely speaking, this approximates to demanding that $m_{H^\pm} < m_t - m_b$ for SM excluded values of m_t, since top decays to real H^+ are very competitive with virtual W^+ modes, whereas decays via virtual H^+ are generally not competitive. Our analysis however is based on exact calculations of the competing H^+ and W^+ channels[12] and we find significant departures from the above approximate statement of the bound on $m_{H^\pm}$.

The $\bar{p}p$ collider experiments have also searched for events with large missing transverse energy (denoted $\not{E}_T$), since this can be a signal for production of SUSY particles or other new physics. It can, in particular, also be a signal for charged-Higgs-boson production because of the undetected neutrinos in $H^+ \to \bar{\tau}\nu \to \bar{\nu}\nu q\bar{q}'$ (or $\bar{\nu}\nu\bar{l}$) decay. Assuming that $H^\pm$ are produced from top-quark decays (the only copious mechanism at hand), upper limits on the frequency of events with large missing E_T will imply constraints on the two-Higgs-doublet model parameters for any given m_t. In this spirit, upper limits on nonstandard contributions with large $\not{E}_T$ from the data of the UA1 experiment[63] at CERN have already been used to set limits[12] on the $H^\pm$ parameters in model II.

The most stringent present limits on top-quark production and on events with large $\not{E}_T$ come from the CDF experiment at the Fermilab Tevatron collider.[16] We use their results to constrain two-Higgs-doublet models.

B. Implications of CDF data

The CDF Collaboration[16] first looked for a top signal based on an isolated charged lepton plus jets, which might arise from $\bar{p}p \to \bar{t}tX$ or $W \to t\bar{b}$ events where only one top quark decays semileptonically. The experimental acceptance for such events varies with m_t and the experimental upper limit on a possible signal therefore also varies with m_t. The theoretical prediction for a signal depends strongly on m_t but also on imprecisely known parton distributions and QCD parameters; we conservatively assume the lowest possible $t\bar{t}$ production cross section[64] in our analysis. The lower bound on m_t is the point where the experimental upper limit and theoretical lower limit cross; currently this gives[16] $m_t \geq 77$ GeV (90% C.L.).

Values of m_t below 77 GeV are excluded unless the SM $t\bar{t}$ signal is suppressed by $B(t \to bW^*)$ having a value less than unity. For a given sign of lepton, say, l^+, this signal arises mainly from $t \to bW^{*+} \to bl^+\nu$ with $\bar{t}$ decaying either via W^{*-} or via H^-. We have calculated that the experimental acceptance for the $W^{*+}H^-$ modes is similar to (and in fact slightly exceeds) that for $W^{*+}W^{*-}$ modes. Hence, the effective bound that can be placed on $B(t \to bW^*)$ is

$$B(t \to bW^*) \leq \left[\frac{\text{experimental } \sigma_{\bar{t}t} \text{ upper limit}}{\text{theory } \sigma_{\bar{t}t} \text{ lower limit}} \right] \equiv R(m_t) . \quad (3.1)$$

This limit is quite conservative; it ignores possible small contributions from $H \to \tau\nu \to l\nu\nu$ decays and the fact that some top quarks are produced from $W \to t\bar{b}$. Reading values of R from the CDF graphs,[16] we obtain approximately

$$B(t \to bW^*) \lesssim 0.28, 0.36, 0.50 \quad \text{for } m_t = 50, 60, 70 \text{ GeV} . \quad (3.2)$$

We calculate this branching fraction as in Ref. 12, for both real- and virtual-Higgs-boson cases, including small contributions such as $t \to sW, sH$ and $H \to us, ub$. The result is insensitive to the precise values of the KM matrix elements, since the dominant channels have matrix elements $\simeq 1$.

The CDF Collaboration also searched for an isolated $e + \mu$ signal, such as might arise from $t\bar{t}$ events where both t and $\bar{t}$ decay semileptonically. These results can be used to derive a second, independent bound similar to Eq. (3.1). However, these constraints are less stringent than Eq. (3.2), so we do not use them here.

The CDF experiment also scanned for events with large $\not{E}_T$ and jets, subject to a stringent set of acceptance cuts designed to remove backgrounds from mismeasured QCD jets, W+jets, etc. For $\not{E}_T \geq 60$ GeV, with an integrated luminosity of 4.6 pb^{-1}, 34 events were observed; the expected background from standard model sources (excluding unknown top decays) is 38 ± 17 events.[16] The latter is not precisely determined because it is derived from observed W and Z event distributions and from heavy-quark Monte Carlo calculations. We treat the background as having a Gaussian probability distribution with mean 38 and standard deviation 17 and derive the bound

$$\sigma(\text{nonstandard physics: } \not{E}_T > 60 \text{ GeV: CDF cuts}) \leq 4.2 \text{ pb} \quad (3.3)$$

at 90% C.L. (see Appendix B). Similarly for $\not{E}_T \geq 40$ GeV, 184 events were observed with expected SM background 158 ± 35 events;[16] from these numbers we derive another bound:

$$\sigma(\text{nonstandard physics: } \not{E}_T > 40 \text{ GeV: CDF cuts}) \leq 16 \text{ pb} \quad (3.4)$$

at 90% C.L. The two missing-E_T bounds are not completely independent since the event samples overlap. Their implied constraints on the model parameters turn out to be rather similar; we therefore illustrate only the $\not{E}_T \geq 60$ GeV bound of Eq. (3.3).

To evaluate the constraints from $\not{E}_T$ bounds, we calculate charged-Higgs-boson production and decay by Monte Carlo methods as in Ref. 12. Conservatively, we evaluate only the dominant $\bar{p}p \to \bar{t}tX$ production by $2 \to 3$

QCD subprocesses (ignoring electroweak $W\to t\bar{b}$ and $gW\to t\bar{b}$ channels that are less important at the Fermilab Tevatron energy) and include top decay via real or virtual W and charged Higgs bosons. For each m_t we normalize our total cross section to the lowest value of the theoretical range in Ref. 64, and simulate the full cascade of decays, coalescing final partons into jets within cones of $\Delta R=[(\Delta\eta)^2+(\Delta\phi)^2]^{1/2}<0.7$, where $\eta=\ln\tan(\theta/2)$ is the pseudorapidity, θ and ϕ are the polar and azimuthal angle with respect to the beam axis. We include standard measurement errors on the lepton and jet E_T, and evaluate the $\not{E}_T$ from the overall transverse energy imbalance. Muons often deposit only a fraction of their energy and thus generate apparent $\not{E}_T$; since this measurement is difficult to simulate accurately, we conservatively ignore events containing muons with $p_T(\mu)>2$ GeV. Finally, we apply CDF acceptance cuts including jet kinematics, multiplicity, and coplanarity, and vetos on hard electron or muon candidates. The resulting cross section for $\not{E}_T>60$ GeV is then compared with the bound of Eq. (3.3).

C. Numerical results

Figure 9 shows the effects of the constraints (3.2) and (3.3) in the $\tan\beta$, $m_{H^\pm}$ plane for model I with $m_t=50,60,70,80$ GeV. In this figure, the regions which lie on the same side of the curves as the cross hatching are excluded. The left-hand margin of this figure, $\tan\beta=0.1$, is approximately the boundary of the perturbative region defined in Eq. (1.5). The lower margin $m_{H^\pm}=25$ GeV is near the present experimental limit.[20] The top-search bound, denoted by solid curves, excludes the upper part of the figure ($m_{H^\pm}\gtrsim m_t$) and also the extreme right-hand side ($\tan\beta\gtrsim 10$) for $m_t\leq 70$ GeV. The missing-E_T constraints, denoted by dashed curves, excludes most of the remaining parameter space, at least for $m_t<70$ GeV [the remaining areas, though not strictly excluded at the level of Eq. (3.3), are nevertheless excluded at 80% confidence level and therefore strongly disfavored for $m_t<70$ GeV].

Figure 10 shows the corresponding bounds in the $\tan\beta$, $m_{H^\pm}$ plane for model II. Again, the areas which are on the cross-hatched side of the curves are excluded. Here the left-hand margin is approximately the perturbative boundary of Eq. (1.5) as before; the right-hand margin $\tan\beta=100$ is approximately the *other* perturbative boundary, where the $\bar{t}bH$ coupling proportional to $m_b\tan\beta$ becomes too large. The top-search bound, denoted by solid curves, lies near $m_{H^\pm}\leq m_t-m_b$ for the middle range of $\tan\beta$ values, but deviates considerably from this value at the extremes (the regions where top decay via *virtual* H becomes competitive). The missing-E_T restrictions,

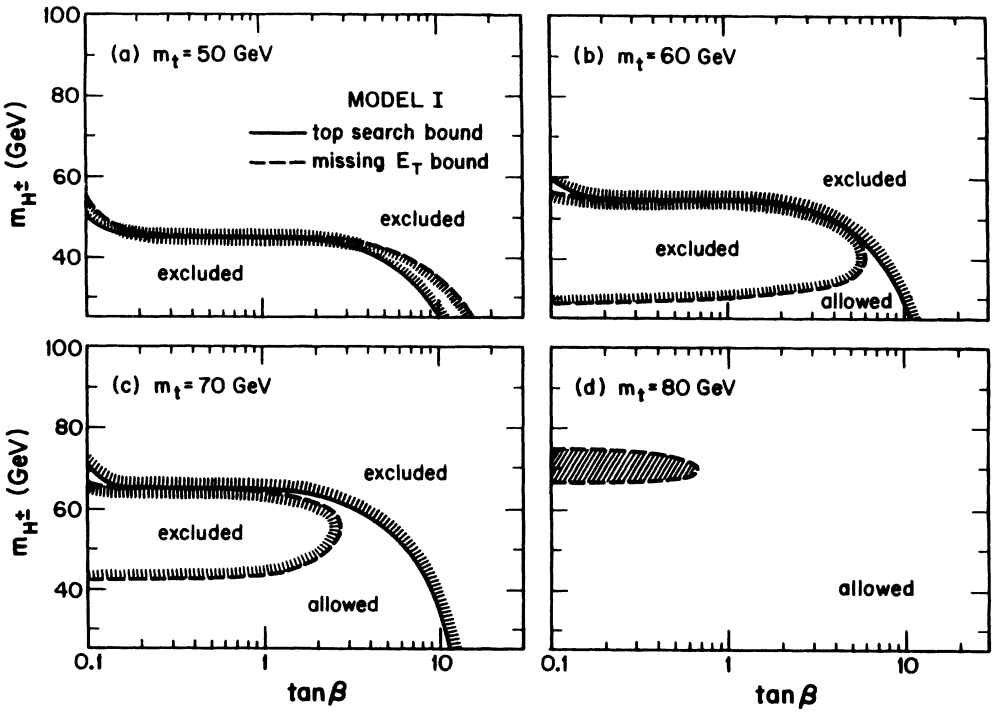

FIG. 9. Constraints in the $(\tan\beta, m_{H^\pm})$ parameter space in model I from the CDF SM top-quark search limits (solid curves) and the CDF missing-E_T bounds (dashed curves) for (a) $m_t=50$ GeV, (b) $m_t=60$ GeV, (c) $m_t=70$ GeV, and (d) $m_t=80$ GeV. The areas which lie on the cross-hatched side of the curves are excluded.

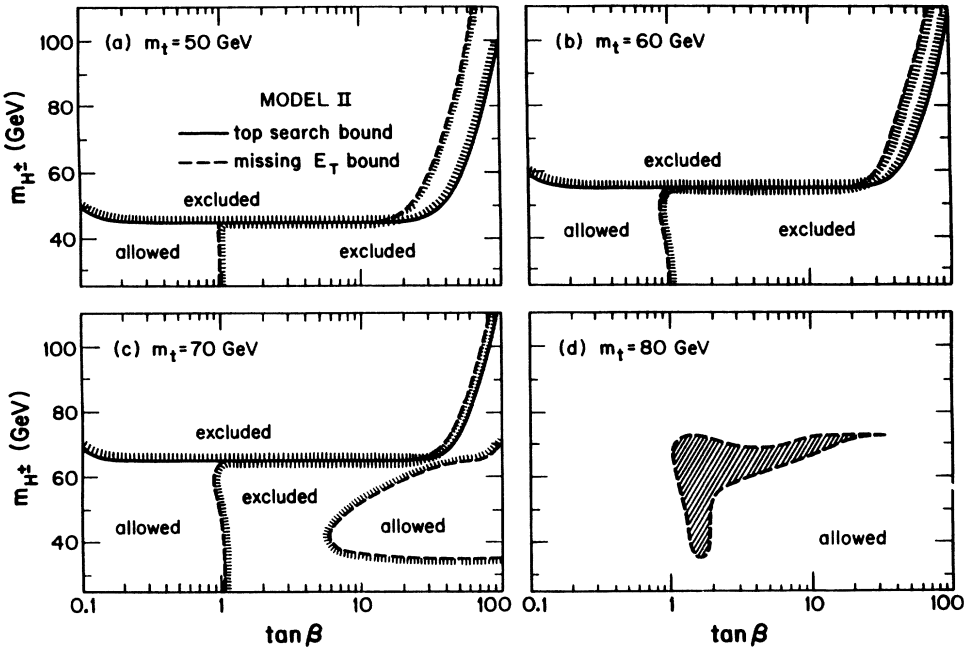

FIG. 10. Constraints in the $(\tan\beta, m_{H^\pm})$ parameter space in model II from the CDF SM top-quark limit search bound (solid curves) and the CDF missing-E_T bounds (dashed curves) for (a) $m_t = 50$ GeV, (b) $m_t = 60$ GeV, (c) $m_t = 70$ GeV, and (d) $m_t = 80$ GeV. The areas which lie on the cross-hatched side of the curves are excluded.

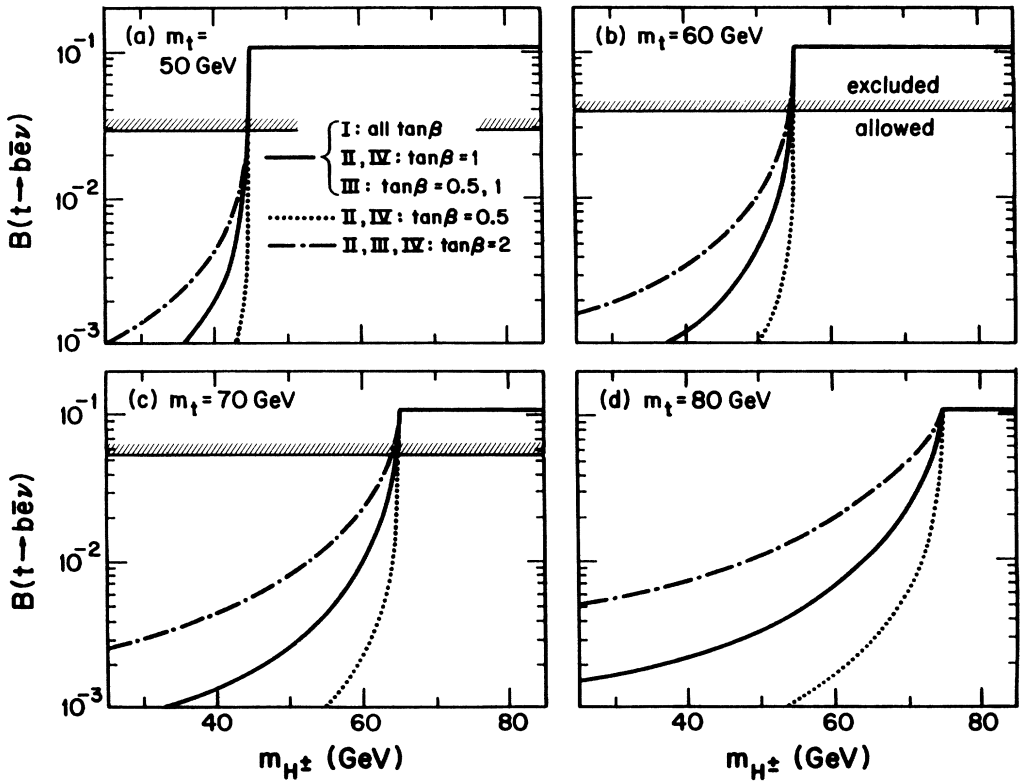

FIG. 11. The branching fraction $B(t \to b\bar{e}\nu)$ vs $m_{H^\pm}$ in various models for (a) $m_t = 50$, (b) $m_t = 60$, (c) $m_t = 70$, (d) $m_t = 80$ GeV. The cross-hatched lines indicate the upper limits from Eq. (3.2), derived from the CDF top search. Solid curves denote model I (all tanβ), models II and IV (tan$\beta = 1$), model III (tan$\beta = 0.5, 1$). Dotted curves denote models II and IV (tan$\beta = 0.5$). Dashed-dotted curves denote models II,III,IV (tan$\beta = 2$).

denoted by dashed curves, excludes essentially all the remaining area for $\tan\beta \gtrsim 1$ with $m_t \leq 70$ [the allowed regions on the right of Fig. 10(c) are technically within the limits but nevertheless again strongly disfavored]. For $m_t = 80$ this constraint is weaker.

The possibility of a "light" top quark with $m_t \leq 70$ GeV and perturbative $\bar{t}bH$ couplings is thus essentially excluded in model I, but survives in model II for $0.1 \lesssim \tan\beta \lesssim 1$. (It has also been shown that a Higgs-triplet representation does not provide[65] enough competition via $t \to H^+ b$ to invalidate the CDF top-quark mass bounds.)

Because charged-Higgs-boson production is dominantly (in our calculation entirely) from top-quark production and decay, the signals get weaker and the experimental limits become less constraining as m_t increases. The missing-E_T bounds in Eqs. (3.3) and (3.4) give weak constraints for $m_t = 80$ GeV and no constraints for $m_t \geq 90$ GeV with our conservative calculations. The top-search bound of Eq. (3.2) is operative only below the SM experimental limit (i.e., for $m_t \leq 77$ GeV at present).

Since the top-search bound depends essentially on the net branching fraction to electrons $B(t \to b\bar{e}\nu)$ and the missing-E_T bound depends on the net branching fraction to taus $B(t \to b\bar{\tau}\nu)$, it is instructive to compare these quantities for models I–IV. Figure 11 shows $B(t \to b\bar{e}\nu)$ vs $m_{H^\pm}$ for $\tan\beta = 0.5, 1.0, 2.0$. Note that all models coincide for $\tan\beta = 1$. The top-quark search limit essentially requires $B < 0.029, 0.039, 0.054$ for $m_t = 50, 60, 70$ GeV, respectively (values indicated by cross-hatched lines in the figure). Models II and IV are equally constrained; model III is similar to model I but *more* strongly restricted at large $\tan\beta$.

Figure 12 shows $B(t \to b\bar{\tau}\nu)$ vs $m_{H^\pm}$ for the same set of $\tan\beta$ values: again all models coincide for $\tan\beta = 1$. The missing-E_T bound, although dependent on other factors too, approximately requires $B < 0.25, 0.30, 0.35, 0.50$ for $m_t = 50, 60, 70, 80$ GeV, respectively (values indicated by cross-hatched lines in the figure). Models II and IV are equally constrained; model III is similar to model I but *less* strongly bounded at large $\tan\beta$.

In technicolor theories of electroweak symmetry breaking, charged technipions have many similarities to the

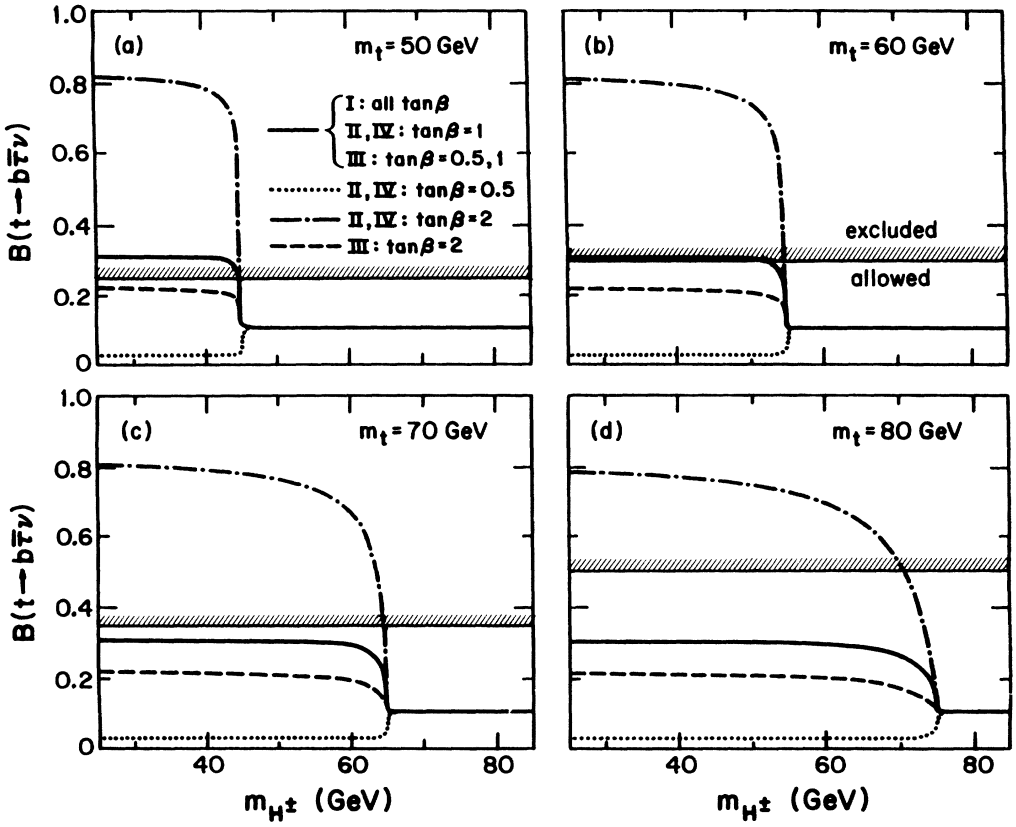

FIG. 12. The branching fraction $B(t \to b\bar{\tau}\nu)$ vs $m_{H^\pm}$ in various models for (a) $m_t = 50$, (b) $m_t = 60$, (c) $m_t = 70$, (d) $m_t = 80$ GeV. The cross-hatched lines indicate approximate upper limits from Eq. (3.3), derived from the CDF missing-E_T bound. Solid curves denote model I (all $\tan\beta$), models II and IV ($\tan\beta = 1$), model III ($\tan\beta = 0.5, 1$). Dotted curves denote models II and IV ($\tan\beta = 0.5$). Dashed-dotted curves denote models II and IV ($\tan\beta = 2$). Dashed curves denote model III ($\tan\beta = 2$).

charged-Higgs-boson scalars of our present analysis. In the models discussed by Godfrey and Holdom,[66] for example, technipions $\pi^{\pm}$ are assumed to have mass less than m_t and are expected to decay dominantly into $\tau\nu$, so that $B(t\to b\pi^+\to b\bar{\tau}\nu)\simeq 1$. In this case our bounds on charged-Higgs-boson parameters from missing E_T can also be used to exclude the range $m_t \lesssim 80$ GeV for this technipion decay mode (and maybe a band of higher t-quark mass also).

IV. CONCLUSIONS

In summary, we have performed a comprehensive analysis of the bounds that low-energy and $\bar{p}p$ collider data place on the parameters of the charged Higgs sector. As can be seen from Fig. 7, the compilation of restrictions of $m_{H^{\pm}}$ and $\tan\beta$ from B_d^0-$\bar{B}_d^0$ and D^0-$\bar{D}^0$ mixing, ΔM_K, ϵ, $|\epsilon'/\epsilon|<5.0\times10^{-3}$, and $b\to s\gamma$ exclude the regions of small $\tan\beta$ and light $m_{H^{\pm}}$ ($\tan\beta\lesssim 0.3$–0.4 and $m_{H^{\pm}}\lesssim 100$–200 GeV, with the precise regions depending on the value of m_t). Slightly stronger constraints are obtained if consistency is demanded (at the $\pm 2\sigma$ level) with the published NA31 data on ϵ'/ϵ. Figures 9 and 10 display the limits that are obtained from the top-quark search and large missing-E_T events at CDF for models I and II. Figure 9 shows that the possible decay $t\to H^+b$ is essentially ruled out in model I for $m_t \lesssim 80$ GeV. In the case of model II, the small region of parameter space which is not restricted by CDF data is exactly the region which is constrained by our low-energy analysis (this can be seen by comparing Figs. 7 and 10). This region is presented in more detail in Fig. 13 where we simultaneously show the constraints in model II from both low-energy and CDF data; only a small sliver in the $m_{H^{\pm}}$,$\tan\beta$ plane survives. Also included in this figure are bounds[21] from the ALEPH detector at LEP from their search for the decay $z\to H^+H^-$.

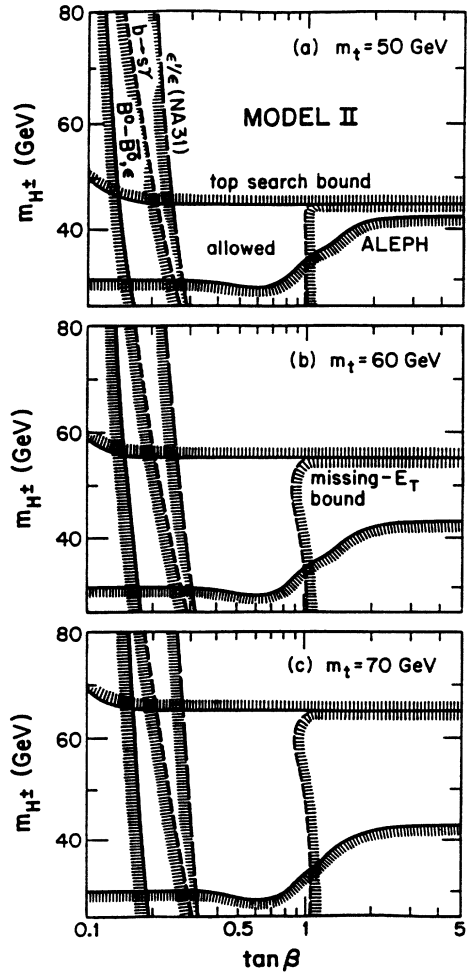

FIG. 13. The overall allowed region in the $m_{H^{\pm}}$,$\tan\beta$ plane for (a) $m_t=50$, (b) $m_t=60$, (c) $m_t=70$ GeV in model II. The thin solid curve indicates the bounds placed from the CDF SM top-quark search; the thin dashed curve from the CDF missing-E_T events; the thick solid curve from B^0-$\bar{B}^0$ and D^0-$\bar{D}^0$ mixing, ΔM_K, ϵ, and $|\epsilon'/\epsilon|<5.0\times10^{-3}$; the thick short-dashed curve from $b\to s\gamma$; and the thick long-dashed curve from ϵ'/ϵ (NA31). The excluded regions lie on the cross-hatched side of the curves.

We have also examined the charged-Higgs-boson contributions to ϵ'/ϵ, $b\to s\gamma$, $K_L\to\mu\mu$, and $K^+\to\pi^+\nu\bar{\nu}$ in both models I and II. We find that the resulting values of ϵ'/ϵ can be negative or positive, and can agree with either the CERN NA31 or Fermilab E731 results, depending on the values of the parameters. The interference between the $H^{\pm}$ and SM contributions to $b\to s\gamma$ in model I and to $K_L\to\mu\mu$ in models I and II can result in substantial enhancements or suppressions over the SM values of these branching fractions. In model II the branching fraction for $b\to s\gamma$ in two-Higgs-doublet models is always enhanced over the SM prediction and can approach the present upper limit. However, the presence of charged Higgs bosons tend to suppress and narrow the range of allowed values for $B(K^+\to\pi^+\nu\bar{\nu})$ as compared to the SM. All of these processes tend to their SM predictions as $\tan\beta$ becomes large.

One of the most important results of our analysis is that the CDF bounds on the top-quark mass can probably not be evaded in either models I or II via the possible decay mode $t\to H^+b$. Model I is already excluded and only a tiny sliver of parameter space remains in model II. Hence the CDF top-mass bound of $m_t>77$ GeV most likely holds in two-Higgs-doublet models as well as in the SM.

The effects of two-Higgs-doublet models are wide and varied. This present study determines the overall regions of the $m_{H^{\pm}}$,$\tan\beta$ parameter space which are consistent with present data and thus helps to pinpoint the best signatures for the possible discovery of charged Higgs bosons.

ACKNOWLEDGMENTS

The authors thank D. Cocolicchio, G. Eilam, S. Geer, J. Flynn, S. Nandi, J. Ng, S. Pakvasa, and T. Rizzo for useful discussions. This research was supported in part by the University of Wisconsin Research Committee with funds granted by the Wisconsin Alumni Research Foun-

dation, and in part by the U.S. Department of Energy under Contract No. DE-AC02-76ER00881.

APPENDIX A: RELEVANT FORMULAS

Here we give the explicit expressions for the functions discussed in the text including, for completeness, those of the SM, which are calculated in Ref. 32.

(i) Box diagrams (model II):

$$A_{WW}(x)=x\left[\frac{1}{4}+\frac{9}{4(1-x)}-\frac{3}{2(1-x)^2}\right]-\frac{3x^3}{2(1-x)^3}\ln x\ , \tag{A1}$$

$$A_{HH}(x,y,z)=x^2[\tfrac{1}{4}I_1(x,y)+z\tan^4\beta\, I_2(x,y)]\ , \tag{A2}$$

$$A_{WH}(x,y,z)=2x^2[I_3(x,y)-\tfrac{1}{4}I_4(x,y)-z\tan^2\beta\, I_3(x,y)]\ , \tag{A3}$$

$$A_{HH}^{cl}(x,y,z)=\tfrac{1}{4}xyI_5(x,y,z)\ , \tag{A4}$$

$$A_{WH}^{cl}(x,y,z)=\tfrac{3}{2}xyI_6(x,y,z)\ . \tag{A5}$$

For model I set $\tan\beta\to 1$ in Eqs. (A2) and (A3). The integrals are given by

$$I_1(x,y)=\frac{x+y}{(x-y)^2}-\frac{2xy}{(x-y)^3}\ln\frac{x}{y}\ , \tag{A6}$$

$$I_2(x,y)=\frac{2}{(x-y)^2}-\frac{x+y}{(x-y)^3}\ln\frac{x}{y}\ , \tag{A7}$$

$$I_3(x,y)=\frac{1}{(x-y)(1-x)}+\frac{y\ln y}{(x-y)^2(1-y)}+\frac{(x^2-y)\ln x}{(x-y)^2(1-x)^2}\ , \tag{A8}$$

$$I_4(x,y)=\frac{x}{(x-y)(1-x)}+\frac{y^2\ln y}{(1-y)(x-y)^2}+\frac{x(x+xy-2y)\ln x}{(x-y)^2(1-x)^2}\ , \tag{A9}$$

$$I_5(x,y,z)=\frac{z}{(x-z)(y-z)}+\frac{y^2\ln y}{(y-x)(y-z)^2}-\frac{x^2\ln x}{(y-x)(x-z)^2}-\frac{(xz+yz-2xy)z\ln z}{(x-z)^2(y-z)^2}\ , \tag{A10}$$

$$I_6(x,y,z)=\frac{y^2\ln y}{(1-y)(y-x)(y-z)}+\frac{x^2\ln x}{(1-x)(x-y)(x-z)}+\frac{z^2\ln z}{(1-z)(z-x)(z-y)}\ . \tag{A11}$$

(ii) ϵ':

$$F_W(x)=\ln x-H(x)\ , \tag{A12}$$

where

$$H(x)=\frac{x^2\ln x}{4(1-x)^4}(15-16x+4x^2)+\frac{x(18-11x-x^2)}{8(1-x)^3}\ , \tag{A13}$$

$$F_H(y)=\frac{-y}{6(1-y)^4}\left[\frac{7y^3}{6}-6y^2+\frac{15y}{2}-\frac{8}{3}+(3y-2)\ln y\right]\ . \tag{A14}$$

(iii) $b\to s\gamma$:

$$G_W(x)=\frac{2-7x+11x^2}{4(1-x)^3}-\frac{1}{2}+\frac{3x^3}{2(1-x)^4}\ln x+Q\left[\frac{1-5x-2x^2}{4(1-x)^3}-\frac{1}{4}-\frac{3x^2}{2(1-x)^4}\ln x\right]\ , \tag{A15}$$

$$G_H^1(y)=\frac{y}{(1-y)^3}\{[\tfrac{1}{2}(1-y^2)+y\ln y]-Q(\tfrac{3}{2}-2y+\tfrac{1}{2}y^2+\ln y)\}\ , \tag{A16}$$

$$G_H^2(y)=\frac{y}{2(1-y)^4}[(\tfrac{1}{6}-y+\tfrac{1}{2}y^2+\tfrac{1}{3}y^3-y^2\ln y)+Q(\tfrac{1}{3}+\tfrac{1}{2}y-y^2+\tfrac{1}{6}y^3+y\ln y)] \tag{A17}$$

with $Q=\frac{2}{3}$, the charge of the internal quark.

(iv) $K_L\to\mu\mu$:

$$C_W(x)=\frac{-2x}{1-x}+\frac{x^2}{2(1-x)}-\frac{3x^2\ln x}{2(1-x)^2}\ , \tag{A18}$$

$$C_H(y)=\frac{-m_t^2}{2M_W^2}\left[\frac{y}{1-y}+\frac{y\ln y}{(1-y)^2}\right]\ . \tag{A19}$$

(v) $K\to\pi\nu\bar{\nu}$:

$$D_{\rm SM}(x_q^W,z_l^W)=-\frac{1}{8}\frac{x_q^Wz_l^W}{z_l^W-x_q^W}\left[\frac{4-z_l^W}{1-z_l^W}\right]^2\ln z_l^W+\frac{1}{4}x_q^W+\frac{3}{8}\left[1-\frac{3}{1-z_l^W}\right]\frac{x_q^W}{1-x_q^W}+\frac{1}{8}\left[\frac{x_q^W}{z_l^W-x_q^W}\left[\frac{4-x_q^W}{1-x_q^W}\right]^2+1+\frac{3}{(1-x_q^W)^2}\right]x_q^W\ln x_q^W\ , \tag{A20}$$

$$D_{ZH}(x_q^W,x_q^H)=-\frac{x_q^W}{4}\left[\frac{x_q^H}{1-x_q^H}+\frac{x_q^H\ln x_q^H}{(1-x_q^H)^2}\right]\ , \tag{A21}$$

$$D_{HH}(x_q^H,z_l^H)=\frac{-m_{H^\pm}^2}{8M_W^2}x_q^H z_l^H\left[\frac{1}{(1-x_q^H)(1-z_l^H)}+\frac{(x_q^H)^2\ln x_q^H}{(1-x_q^H)^2(x_q^H-z_l^H)}+\frac{(z_l^H)^2\ln z_l^H}{(1-z_l^H)^2(z_l^H-x_q^H)}\right], \tag{A22}$$

$$\begin{aligned}D_{WH}\left[x_q^W,z_l^W,w\equiv\frac{m_{H^\pm}^2}{M_W^2}\right]=x_q^W z_l^W\Bigg[&\frac{x_q^W\ln x_q^W}{(1-x_q^W)(z_l^W-x_q^W)(w-x_q^W)}+\frac{z_l^W\ln z_l^W}{(1-z_l^W)(x_q^W-z_l^W)(w-z_l^W)}\\&+\frac{w\ln w}{(1-w)(z_l^W-w)(x_q^W-w)}\\&+\frac{1}{4}\left[\frac{(x_q^W)^2\ln x_q^W}{(1-x_q^W)(z_l^W-x_q^W)(w-x_q^W)}\right.\\&\left.+\frac{(z_l^W)^2\ln z_l^W}{(1-z_l^W)(x_q^W-z_l^W)(w-z_l^W)}+\frac{w^2\ln w}{(1-w)(z_l^W-w)(x_q^W-w)}\right]\Bigg].\end{aligned} \tag{A23}$$

APPENDIX B: CROSS-SECTION CONFIDENCE LIMITS

Suppose N events have been seen, with known background B (i.e., B = mean number of expected background events). The probability that n_B of the observed N events were due to background has Poisson distribution:

$$\text{Prob}(B:n_B)=\frac{e^{-B}B^{n_B}}{n_B!}\Big/\left[\sum_{n=0}^{N}\frac{e^{-B}B^n}{n!}\right]. \tag{B1}$$

Here the factor in large parentheses arises because *we already know* that n_B cannot exceed N, so the sum of probabilities for $n_B\le N$ must be 1. For a given signal S (= mean number of expected signal events), the probability that n_S signal events were seen has Poisson distribution

$$\text{Prob}(S:n_S)=e^{-S}S^{n_S}/n_S! \tag{B2}$$

Since we do not know (conservatively) that any signal is present at all, the sum of probabilities for $n_S\le N$ is not normalized to 1 here (although if $S\ll N$ this will be approximately the case). For given N,B,S the probability that the observed number of events should not have exceeded N is then conservatively estimated by folding these distributions together (see, e.g., Ref. 37, Eq. II.28 and accompanying discussion):

$$\text{Prob}(B,S:n_B+n_S\le N)=\left[\sum_{n=0}^{N}\frac{e^{-(B+S)}(B+S)^n}{n!}\right]\Big/\left[\sum_{n=0}^{N}\frac{e^{-B}B^n}{n!}\right], \tag{B3}$$

and the confidence level with which this value of S can be excluded is 1 minus this probability. In our present work B is not precisely known, but a mean value B_0 and standard deviation ΔB are given. We therefore take B to have a continuous Gaussian probability distribution with these parameters. Since B cannot be negative we restrict it to the range $0\le B\le 2B_0$ (which is conservative and also ensures that the mean value remains at B_0), with Gaussian weight $\sim\exp[-\frac{1}{2}(B-B_0)^2/(\Delta B)^2]$ normalized to 1 in this range. We then replace the right-hand side of Eq. (B3) by the Gaussian weighted mean and take the corresponding confidence level.

[1]For a recent review of the status of the SM, see R. Barbieri, plenary talk given at International Europhysics Conference on High Energy Physis, Madrid, Spain, 1989 (unpublished).

[2]For a recent review of the minimal Higgs sector and its possible extensions, see J. F. Gunion, H. E. Haber, G. L. Kane, and S. Dawson, *The Higgs Hunter's Guide* (Addison-Wesley, Reading, MA, 1989).

[3]H. Haber and G. Kane, Phys. Rep. **117**, 75 (1985).

[4]R. D. Peccei and H. R. Quinn, Phys. Rev. D **16**, 1791 (1977); Phys. Rev. Lett. **38**, 1440 (1977); S. Weinberg, *ibid.* **40**, 223 (1978); F. Wilczek, *ibid.* **40**, 279 (1978).

[5]T. D. Lee, Phys. Rev. D **8**, 1226 (1973); G. C. Branco, A. J. Buras, and J.-M. Gerard, Nucl. Phys. **B259**, 306 (1985); J. Liu and L. Wolfenstein, *ibid.* **B272**, 145 (1986).

[6]For a recent review, see J. L. Hewett and T. G. Rizzo, Phys. Rep. **183**, 193 (1989).

[7]S. L. Glashow and E. E. Jenkins, Phys. Lett. B **196**, 223 (1987); F. Hoogeveen and C. N. Leung, Phys. Rev. D **37**, 3340 (1988); G. Altarelli and P. J. Franzini, Z. Phys. C **37**, 271 (1988).

[8]L. F. Abbott, P. Sikivie, and M. B. Wise, Phys. Rev. D **21**, 1393 (1980); G. G. Athanasiu and F. J. Gilman, Phys. Lett. **153B**, 274 (1985); G. G. Anthanasiu, P. J. Franzini, and F. J. Gilman, Phys. Rev. D **32**, 3010 (1985).

[9]P. A. deSousa Gerbert, Nucl. Phys. **B272**, 581 (1986).

[10]C. Q. Geng and J. N. Ng, Phys. Rev. D **38**, 2858 (1988); G. Bélanger *et al.*, in *High Energy Physics in the 1990's*, proceedings, Snowmass, Colorado, 1988, edited by S. Jensen (World Scientific, Teaneck, 1989).

[11]T. G. Rizzo, Phys. Rev. D **38**, 820 (1988); B. Grinstein and M. B. Wise, Phys. Lett. B **201**, 274 (1988); W.-S. Hou and R. S. Willey, *ibid.* **202**, 591 (1988); T. D. Nguyen *et al.*, Phys. Rev. D **37**, 3220 (1988); D. Ciuchini, Mod. Phys. Lett. A **4**, 1945 (1989).

[12]V. Barger and R. J. N. Phillips, Phys. Lett. B **201**, 553 (1988); Phys. Rev. D **41**, 894 (1990).

[13]P. Krawczyk and S. Pokorski, Phys. Rev. Lett. **60**, 182 (1988).

[14]J. L. Hewett, S. Nandi, and T. G. Rizzo, Phys. Rev. D **39**, 250 (1989), and erratum (to be published).

[15]After this work was completed we received related reports from A. Buras, P. Krawczyk, M. E. Lautenbacker, and C. Salazar, Max Planck Institute Report No. MPI-PAE/PTh52/89, 1989 (unpublished); J. F. Gunion and B. Grzadkowski, University of California–Davis Report No. UCD-89-30, 1989 (unpublished).

[16]CDF Collaboration, F. Abe *et al.*, Phys. Rev. Lett. **64**, 142 (1990); L. Nodulman, plenary talk given at International Europhysics Conference on High Energy Physics (Ref. 1); J. Freeman, report presented at Les Rencontres de la Vallée d'Aoste, 1989 (unpublished).

[17]M. Kobayashi and T. Maskawa, Prog. Theor. Phys. **49**, 673 (1973).

[18]S. Glashow and S. Weinberg, Phys. Rev. D **15**, 1958 (1977); E. A. Paschos, *ibid.* **15**, 1966 (1977).

[19]M. Olechowski and S. Pokorski, Phys. Lett. B **214**, 393 (1988).

[20]CELLO Collaboration, H. J. Behrends *et al.*, Phys. Lett. B **193**, 376 (1987).

[21]ALEPH Collaboration, D. Decamp *et al.*, Phys. Lett. B **236**, 233 (1990); S.-L. Wu (talk given at Aspen Winter Conference, Aspen, Colorado, 1990) (unpublished).

[22]J. F. Gunion and H. E. Haber, Nucl. Phys. **B272**, 1 (1986); **B278**, 449 (1986).

[23]V. Barger and K. Whisnant, Int. J. Mod. Phys. A **3**, 1907 (1988); also J. F. Gunion, L. Roszkowski, and H. E. Haber, Phys. Rev. D **38**, 105 (1988).

[24]T. G. Rizzo, Phys. Lett. B **237**, 88 (1990).

[25]S. Bertolini, Nucl. Phys. **B272**, 77 (1986); W. Hollik, Z. Phys. C **32**, 291 (1986); **37**, 569 (1988); L. Alvarez-Gaumé, J. Polchinski, and M. Wise, Nucl. Phys. **B221**, 495 (1983); C. S. Lim, T. Inami, and N. Sakai, Phys. Rev. D **29**, 1488 (1984); G. Passarino, Phys. Lett. B **231**, 458 (1989); M. Veltman, Nucl. Phys. **B123**, 89 (1977); S. R. Moore, B.-L. Young, and K. Whisnant, Phys. Rev. D **37**, 179 (1988).

[26]T. G. Rizzo (private communication).

[27]Mark II Collaboration, G. S. Abrams *et al.*, Phys. Rev. Lett. **63**, 2447 (1989).

[28]OPAL Collaboration, M. Z. Akrawy *et al.*, Phys. Lett. B **236**, 364 (1990).

[29]R. Foot, H. Lew, and G. C. Joshi, University of Melbourne Report No. UM-P-88/53, 1988 (unpublished).

[30]H. Schroder, in *Proceedings of the XXIV International Conference on High Energy Physics,* Munich, West Germany, 1988, edited by R. Kotthaus and J. Kuhn (Springer, Berlin, 1988).

[31]F. Gilman and M. Wise, Phys. Rev. D **27**, 1128 (1983); W. A. Kaufman, H. Steger, and Y.-P. Yao, Mod. Phys. Lett. A **3**, 1479 (1988); J. M. Flynn, Rutherford Appleton Laboratory Report No. RAL-89-093, 1989 (unpublished); E. A. Paschos, T. Schneider, and Y. L. Wu, University of Dortmund Report No. DO-TH 89/10, 1989 (unpublished).

[32]T. Inami and C. S. Lim, Prog. Theor. Phys. **65**, 297 (1981).

[33]L.-L. Chau and W.-Y. Keung, Phys. Rep. **95**, 1 (1983).

[34]G. Altarelli and P. J. Franzini, talk given at Symposium on Present Trends, Concepts, and Instruments of Particle Physics, Rome, Italy, 1987 (unpublished).

[35]C. Bernard *et al.*, Phys. Rev. D **38**, 3540 (1988); H. W. Hamber, *ibid*, **39**, 896 (1989); M. B. Gavela *et al.*, Phys. Lett. B **206**, 113 (1988); C. Bernard and A. Soni, in *Lattice '88,* proceedings of the International Symposium, Batavia, Illinois, 1988, edited by A. S. Kronfeld and P. B. Mackenzie [Nucl. Phys. B (Proc. Suppl.) **9**, (1989)].

[36]Tagged Photon Spectrometer Collaboration, J. C. Anjos *et al.*, Phys. Rev. Lett. **60**, 1239 (1988); E615 Collaboration, W. C. Louis *et al.*, *ibid.* **56**, 1027 (1988).

[37]Particle Data Group, G. P. Yost *et al.*, Phys. Lett. B **204**, 1 (1988).

[38]A. Datta and D. Kumbhaker, Z. Phys. C **27**, 515 (1985); H.-Y. Cheng, Phys. Rev. D **26**, 143 (1982).

[39]L. Wolfenstein, Phys. Lett. **164B**, 170 (1985); J. Donoghue *et al.*, Phys. Rev. D **33**, 179 (1986).

[40]For a recent review, see J.-M. Gérard, talk presented at the 12th Warsaw Symposium on Elementary Particle Physics, Kazimierz, Poland, 1989 (unpublished).

[41]For example, see G. Beall, M. Bander, and A. Soni, Phys. Rev. Lett. **48**, 848 (1982).

[42]E. A. Paschos and U. Turke, Phys. Rep. **178**, 147 (1989).

[43]A. J. Buras, in *Proceedings of International Europhysics Conference on High Energy Physics,* Bari, Italy, 1985, edited by L. Nitti and G. Preparata (Laterza, Bari, 1985).

[44]T. Devlin and J. Dickey, Rev. Mod. Phys. **54**, 237 (1979).

[45]B. Guberina and R. D. Peccei, Nucl. Phys. **B163**, 289 (1980).

[46]A. I. Vainshtein, V. I. Zakharov, and M. A. Shifman, Zh. Eksp. Teor. Fiz. **73**, 1271 (1977) [Sov. Phys. JETP **45**, 669 (1977)].

[47]J. Gasser and H. Leutwyler, Phys. Rep. **87**, 77 (1982).

[48]NA31 Collaboration, H. Burkhardt *et al.*, Phys. Lett. B **206**, 169 (1988).

[49]B. Winstein, in *Proceedings of the 14th International Symposium on Lepton and Photon Interactions,* Stanford, California, 1989, edited by M. Riordan (World Scientific, Singapore, in press).

[50]J. M. Flynn and L. Randall, Phys. Lett. B **224**, 221 (1989).

[51]X.-G. He, B. H. M. McKellar, and S. Pakvasa, Int. J. Mod. Phys. A **4**, 5011 (1989).

[52]A. Soni, in *Proceedings of the B-Meson Factory Workshop,* Stanford, California, 1987, edited by L. Friedsam (SLAC Report No. 324, Stanford, 1988).

[53]N. G. Deshpande *et al.*, Phys. Rev. Lett. **59**, 183 (1987); S. Bertolini, F. Borzumati, and A. Masiero, *ibid.* **59**, 180 (1987); B. Grinstein, R. Springer, and M. B. Wise, Phys. Lett. B **202**, 138 (1988).

[54]ARGUS Collaboration, H. Schulz, in *Proceedings of the Second Symposium on the Fourth Family of Quarks and Leptons,* Santa Monica, California, 1989, edited by D. Cline and A. Soni (New York Academy of Sciences, New York, 1989); CLEO Collaboration, N. Mistry, *ibid.*; ARGUS Collaboration, M. V. Danilov, in *Proceedings of the 14th International Symposium on Lepton and Photon Interactions* (Ref. 49); CLEO Collaboration, D. L. Kreinick, *ibid.*

[55]N. G. Deshpande, P. Lo, and J. Trampetic, Z. Phys. C **40**, 369 (1988).

[56]T. Inagaki *et al.*, Phys. Rev. D **40**, 1712 (1989); C. Mathiazhagan *et al.*, Phys. Rev. Lett. **63**, 2185 (1989).

[57]C. Q. Geng and J. N. Ng, Phys. Rev. D **41**, 2351 (1990); L. M. Sehgal, Phys. Rev. **183**, 1511 (1969).

[58]V. Barger, W. F. Long, E. Ma, and A. Pramudita, Phys. Rev. D **25**, 1860 (1982).

[59]J. Ellis and J. S. Hagelin, Nucl. Phys. **B217**, 189 (1983); C. O. Dib, I. Dunietz, and F. J. Gilman, Report No. SLAC-PUB-4840-T, 1989 (unpublished).

[60]L. Littenburg, in *Proceedings of the 14th International Symposium on Lepton and Photon Interactions* (Ref. 49).

[61]G. Eilam *et al.*, Phys. Rev. D **34**, 2790 (1986); Phys. Lett. B **193**, 533 (1987); J. L. Hewett, *ibid.* **193**, 327 (1987).

[62]See, for example, UA1 Collaboration, P. Sinervo, in *Proceedings of the 14th International Symposium on Lepton and Pho-*

ton Interactions (Ref. 49); UA2 Collaboration, L. di Lella, *ibid.*; CDF Collaboration, P. Sinervo, *ibid.*

[63]UA1 Collaboration, C. Albajar *et al.*, Phys. Lett. B **185**, 233 (1987).

[64]G. Altarelli *et al.*, Nucl. Phys. **B308**, 724 (1988).

[65]T. G. Rizzo, Phys. Rev. D **41**, 1504 (1990).

[66]S. Godfrey and B. Holdom, Phys. Lett. B **233**, 236 (1989).